eng

MDPI

Review

Proton Exchange Membrane Electrolysis Revisited: Advancements, Challenges, and Two-Phase Transport Insights in Materials and Modelling

Ali Bayat [1], Prodip K. Das [2], Goutam Saha [1,3,4,*] and Suvash C. Saha [1,*]

[1] School of Mechanical and Mechatronic Engineering, University of Technology Sydney, Sydney, NSW 2007, Australia; ali.bayat@student.uts.edu.au
[2] School of Engineering, The University of Edinburgh, Edinburgh EH9 3BF, UK; prodip.das@ed.ac.uk
[3] Miyan Research Institute, International University of Business Agriculture and Technology, Dhaka 1230, Bangladesh
[4] Department of Mathematics, University of Dhaka, Dhaka 1000, Bangladesh
* Correspondence: goutam.saha@uts.edu.au (G.S.); Suvash.Saha@uts.edu.au (S.C.S.)

Abstract: The transition to clean energy has accelerated the pursuit of hydrogen as a sustainable fuel. Among various production methods, proton exchange membrane electrolysis cells (PEMECs) stand out due to their ability to generate ultra-pure hydrogen with efficiencies exceeding 80% and current densities reaching 2 A/cm^2. Their compact design and rapid response to dynamic energy inputs make them ideal for integration with renewable energy sources. This review provides a comprehensive assessment of PEMEC technology, covering key internal components, system configurations, and efficiency improvements. The role of catalyst optimization, membrane advancements, and electrode architectures in enhancing performance is critically analyzed. Additionally, we examine state-of-the-art numerical modelling, comparing zero-dimensional to three-dimensional simulations and single-phase to two-phase flow dynamics. The impact of oxygen evolution and bubble dynamics on mass transport and performance is highlighted. Recent studies indicate that optimized electrode architectures can enhance mass transport efficiency by up to 20%, significantly improving PEMEC operation. Advancements in two-phase flow simulations are crucial for capturing multiphase transport effects, such as phase separation, electrolyte transport, and membrane hydration. However, challenges persist, including high catalyst costs, durability concerns, and scalable system designs. To address these, this review explores non-precious metal catalysts, nanostructured membranes, and machine-learning-assisted simulations, which have demonstrated cost reductions of up to 50% while maintaining electrochemical performance. Future research should integrate experimental validation with computational modelling to improve predictive accuracy and real-world performance. Addressing system control strategies for stable PEMEC operation under variable renewable energy conditions is essential for large-scale deployment. This review serves as a roadmap for future research, guiding the development of more efficient, durable, and economically viable PEM electrolyzers for green hydrogen production.

Keywords: PEM electrolysis; hydrogen production; multiphysics modelling; catalyst development; renewable energy; numerical simulation

Academic Editor: Qiuwan Shen

Received: 10 March 2025
Revised: 27 March 2025
Accepted: 2 April 2025
Published: 4 April 2025

Citation: Bayat, A.; Das, P.K.; Saha, G.; Saha, S.C. Proton Exchange Membrane Electrolysis Revisited: Advancements, Challenges, and Two-Phase Transport Insights in Materials and Modelling. *Eng* **2025**, *6*, 72. https://doi.org/10.3390/eng6040072

1. Introduction

Hydrogen has garnered significant attention as an energy carrier in response to escalating global air pollution. Recognized for its cleanliness and versatility, it serves as a promising energy source capable of providing heat and power across various sectors [1,2]. As the most abundant element in the universe, hydrogen's applications span clean energy, renewable storage, transportation decarbonization, industrial use, and more [3,4]. Advancing green hydrogen is essential for enabling low-temperature fuel cells as viable alternatives to battery electric systems in combating climate change [5].

Hydrogen does not naturally exist in its diatomic molecular form and must be synthesized using energy sources such as fossil fuels. Common methods include steam reforming of methane at high temperatures [6], gasification [7], and even emerging approaches like thermo-catalytic plastic waste conversion [8]. Natural gas, rich in methane, remains a key feedstock, reacting with steam (700–1000 °C) to yield hydrogen [9] through the following steps:

$$\begin{gathered}\text{Steam-methane reforming: } CH_{4\,(g)} + H_2O_{\,(g)} \rightarrow CO_{\,(g)} + 3H_{2\,(g)} \\ \text{Water-gas shift: } CO_{\,(g)} + H_2O_{\,(g)} \rightarrow CO_{2\,(g)} + H_{2\,(g)} + \text{Heat}\end{gathered} \quad (1)$$

Hydrogen is often classified by its production method: grey (from fossil fuels, emits CO_2), blue (uses CCS), and green (via electrolysis using renewables) [10,11]. Green hydrogen is the most environmentally friendly. Electrolysis splits water into hydrogen and oxygen using electricity [12]:

$$2H_2O_{\,(l)} + \text{Electricity} \rightarrow 2H_{2\,(g)} + O_{2\,(g)} \quad (2)$$

Among all current methods for hydrogen production via water electrolysis, proton exchange membrane electrolysis cells (PEMECs) have emerged as a leading technology due to their ability to deliver high-purity hydrogen, operate at elevated current densities, respond swiftly to fluctuating energy inputs, and maintain a compact, scalable design [13–15].

This review provides a focused evaluation of numerical simulation approaches aimed at enhancing PEMEC performance, with an emphasis on advancements in modelling techniques and their practical applications. It covers a range of computational models—from zero-dimensional to fully three-dimensional frameworks and from single-phase to multiphase simulations—analyzing outputs such as polarization curves, efficiency predictions, and multiphysics coupling [13–16]. Through critical analysis of these methods, this review identifies key strengths, limitations, and research gaps that require further refinement to improve predictive accuracy and support experimental validation.

A key novelty of this work lies in its integrated approach, linking recent material developments—including membrane innovations, catalyst architectures, and porous transport layers—with their direct influence on numerical simulation results. Unlike prior reviews that treat materials and simulations independently, this study emphasizes the mutual dependency between material properties and modelling accuracy, showing how simulations can also guide future material design and system-level optimization.

Furthermore, this review delves into advanced multiphysics and two-phase flow models, which are essential to understanding internal PEMEC transport dynamics. Recent 3D, non-isothermal, two-phase studies have provided valuable insights into gas–liquid interactions, electrochemical kinetics, and spatial mass transport—crucial for optimizing PEMECs at high-current densities for commercial applications.

To support this modelling emphasis, this paper explores how material configurations and component properties—such as membrane conductivity, catalyst layer porosity, and flow-field geometry—affect simulation fidelity and real-world performance [17–21]. In doing so, it highlights emerging challenges, such as the need for validated two-phase

models, scalable catalyst structures, and high-fidelity numerical frameworks that balance accuracy and computational cost.

This review is structured to deliver a comprehensive and systematic overview of PEMEC simulation research. Section 2 introduces the fundamentals of water electrolysis, comparing key hydrogen production technologies. Section 3 outlines the core governing equations used in PEMEC modelling, while Section 4 examines critical components—including membranes, catalysts, and flow fields—and their role in cell behaviour.

Building on this foundation, Section 5 discusses modern numerical approaches from low- to high-dimensional models and from single-phase to two-phase simulation strategies. Section 6 evaluates flow-field modelling and the trade-offs between simulation accuracy and computational demand. Section 7 compares single-phase and two-phase PEMEC models, emphasizing the importance of capturing detailed transport phenomena such as gas evolution, velocity fields, and pressure distribution. This is supported by benchmarking results against experimental data, highlighting the value of two-phase modelling in replicating real-world behaviour.

This paper concludes with Section 8, which summarizes the key findings and research directions for advancing PEMEC scalability and performance, followed by Section 9, which discusses current limitations and the need for further model validation, particularly under dynamic operating conditions.

By connecting modelling advancements with material innovation and system optimization, this review aims to provide a comprehensive roadmap for the development of cost-effective, efficient, and scalable PEMEC technologies for green hydrogen production.

2. Hydrogen Production by Water Electrolysis

Water electrolysis is one of the most promising technologies for large-scale hydrogen production, offering a direct pathway to clean energy. However, different electrolysis methods vary significantly in efficiency, cost, and operational complexity. This section examines four widely used approaches—alkaline water electrolysis cell (AWE), molten carbonate electrolysis (MCE), solid oxide electrolysis (SOEC), and proton exchange membrane (PEM) electrolysis—comparing their characteristics, advantages, and limitations to assess their suitability for sustainable hydrogen production [22].

The schematic illustrations of these four electrolysis methods are presented in Figure 1, providing visual insight into their structural and operational differences. These electrolysis technologies differ mainly in the type of electrolyte used, operating temperature, dynamic response, and integration capability with renewable sources. While AWE remains the most established due to its low cost and durability, it suffers from low-current densities and gas crossover issues. MCE is notable for co-producing CO and supporting carbon capture applications, yet it operates at very high temperatures and poses corrosion challenges. SOECs are highly efficient and suitable for waste heat recovery, though they require complex ceramic components and face durability issues. PEM electrolysis, by contrast, offers high purity, a fast response, and a compact design, making it attractive for renewable coupling, but is limited by a high capital cost and catalyst degradation.

Given that detailed operational principles, reaction mechanisms, and cell architectures of these technologies are widely available in textbooks and previous review articles, a comparative summary of their key characteristics is presented in Table 1.

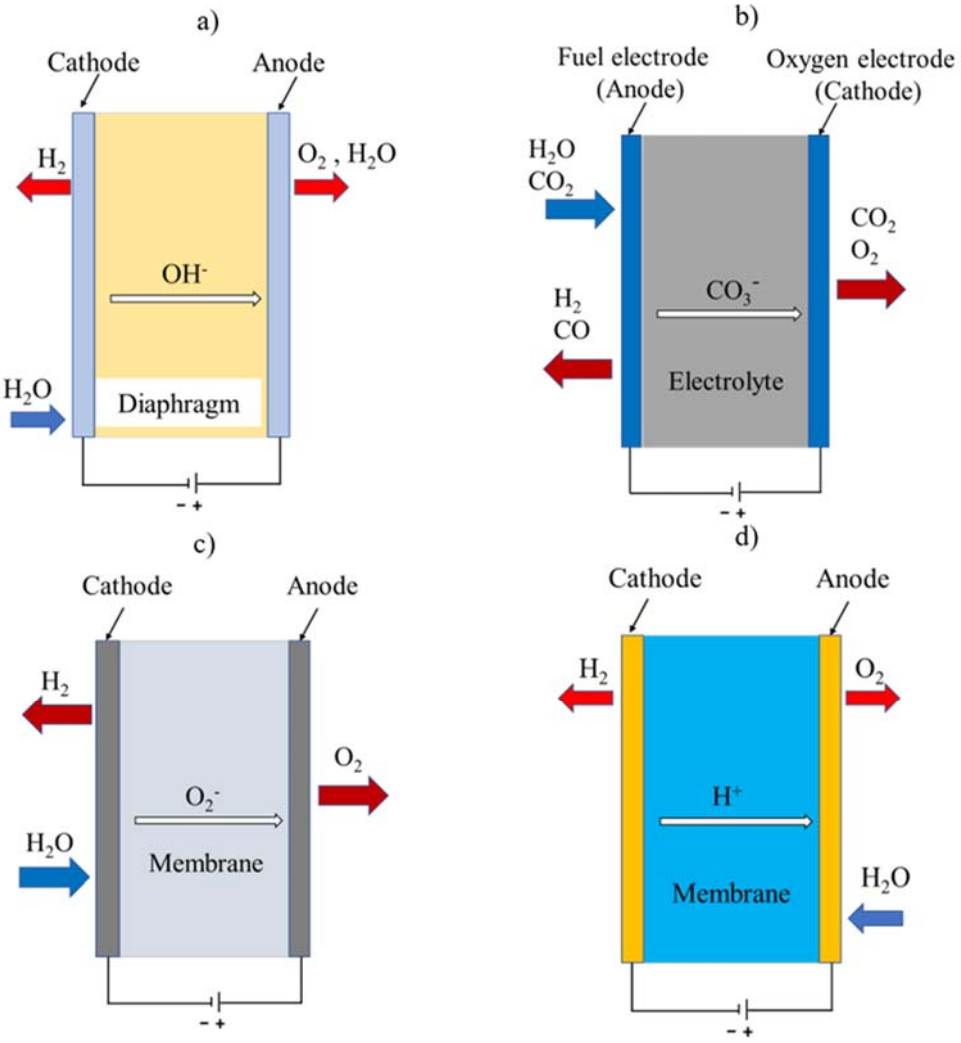

Figure 1. Schematic of the four main electrolysis methods: (**a**) AWE using a KOH electrolyte with nickel-based electrodes; (**b**) MCE capturing CO_2 and producing syngas; (**c**) SOEC operating at high temperatures to leverage waste heat; (**d**) PEMEC utilizing a proton-conducting membrane for high-efficiency hydrogen production.

Table 1. Summary of electrolysis technologies for hydrogen production.

Technology	Electrolyte	Temp (°C)	Key Advantages	Key Challenges	References
AWE	KOH (20–30%)	60–90	Low cost, mature, durable	Low-current density, poor load response	[4,22]
MCE	Molten Li2CO3/K2CO3	650–700	CO production, carbon capture	Corrosive, high energy demand	[23,24]
SOEC	Solid ceramic oxide	600–850	High efficiency, waste heat integration	Material degradation, sealing complexity	[4,25]
PEMEC	Solid polymer membrane	50–80	High purity, fast response, compact	High cost, catalyst/membrane degradation	[13–16]

While each electrolysis method offers distinct benefits, PEM electrolysis has received particular attention due to its compatibility with renewable energy, compact design, and high hydrogen purity. In this method, a solid polymer membrane facilitates proton transfer while blocking electrons, enabling safe and efficient hydrogen production at moderate temperatures [13–16]. Despite its high efficiency—exceeding 80% in some cases—PEMECs face persistent challenges, including catalyst degradation and membrane durability under

prolonged or fluctuating operation. The reactions that happen at the anode and cathode compartment are stated in Equation (3) [4]:

$$\begin{aligned} 2H_2O_{(l)} \rightarrow O_{2(g)} + 4H^+ + 4e^- \quad & \text{Anode } (V_{anode}=1.23\ V) \\ 4H^+ + 4e^- \rightarrow 2H_{2(g)} \quad & \text{Cathode } (V_{cathode}=0\ V) \end{aligned} \tag{3}$$

Although the core reactions are straightforward, the overall system performance is heavily influenced by component design, such as membrane conductivity, catalyst structure, and porous transport layers (PTLs). These internal features govern mass transport, reaction kinetics, and long-term efficiency. Despite these technological advancements, PEMECs face key operational and economic challenges that impact their widespread adoption. The following section examines both the advantages and challenges of PEMEC technology, providing a balanced assessment of its current status and future prospects.

3. Advantages and Challenges of PEMECs

PEMECs offer distinct advantages, including high-purity hydrogen production, rapid system response, and compact design—features that make them especially attractive for integration with renewable energy systems [3,4,13–16,26,27]. However, these benefits are offset by challenges such as high system costs, the reliance on noble metal catalysts, and the need for precise water and contaminant control [4,28–30]. While PEMECs have strong potential for clean hydrogen generation, their economic competitiveness remains limited, particularly for large-scale deployment. The dependence on expensive and scarce materials like iridium and platinum introduces cost and supply chain vulnerabilities [31]. Several studies have explored material substitution and structural modifications, but few have demonstrated long-term stability or validated their findings through predictive modelling, highlighting a persistent gap between experimental development and simulation-based design. Another critical barrier is performance degradation under dynamic loading, especially when powered by intermittent renewables. Cyclic operation accelerates wear in membranes, catalyst layers, and PTLs, reducing efficiency and lifespan [4]. Although these degradation trends are well-documented experimentally, existing models rarely capture transient mechanical or electrochemical deterioration, limiting their applicability for real-world system forecasting. Performance benchmarks reported by Millet et al. [32]—such as 2 A/cm^2 at 2.1 V and hydrogen output below 10 Nm^3/h—illustrate PEMECs' potential. However, most models assume steady-state conditions and ignore temporal effects, making it difficult to evaluate durability or system behaviour under fluctuating inputs. In comparing PEMEC to AWE, Smolinka et al. [33] noted that while the latter is more cost-effective at scale, PEMECs deliver superior hydrogen quality and responsiveness. These features, however, introduce additional multiphysics modelling requirements, such as coupled gas-liquid transport, thermal effects, and transient boundary conditions—factors often simplified or excluded in current simulations. To address performance limitations, recent studies have proposed innovations at the component level. Advanced manufacturing techniques like atomic layer deposition (ALD) have shown promise in reducing precious metal use while maintaining catalyst activity [34]. Kang et al. [35] developed a tuneable, ultra-thin PTL to improve mass transport and reduce ohmic losses, and Thumbarathy et al. [34] demonstrated the benefits of optimizing porosity and permeability in fuel cells. Despite encouraging experimental data, these component innovations are rarely incorporated into detailed numerical models, leaving their long-term viability underexplored.

4. Components, Functions, and Performance of PEMECs

A PEMEC consists of several key components that collectively determine its performance, efficiency, and durability. The core of a PEMEC is the membrane electrode assembly (MEA), which includes a proton-conducting membrane, catalyst CLs, and PTLs. Structural components such as bipolar plates (BPs), gaskets, current collectors, and end plates provide mechanical stability and ensure efficient operation. Figure 2 provides a schematic representation of the PEMEC structure.

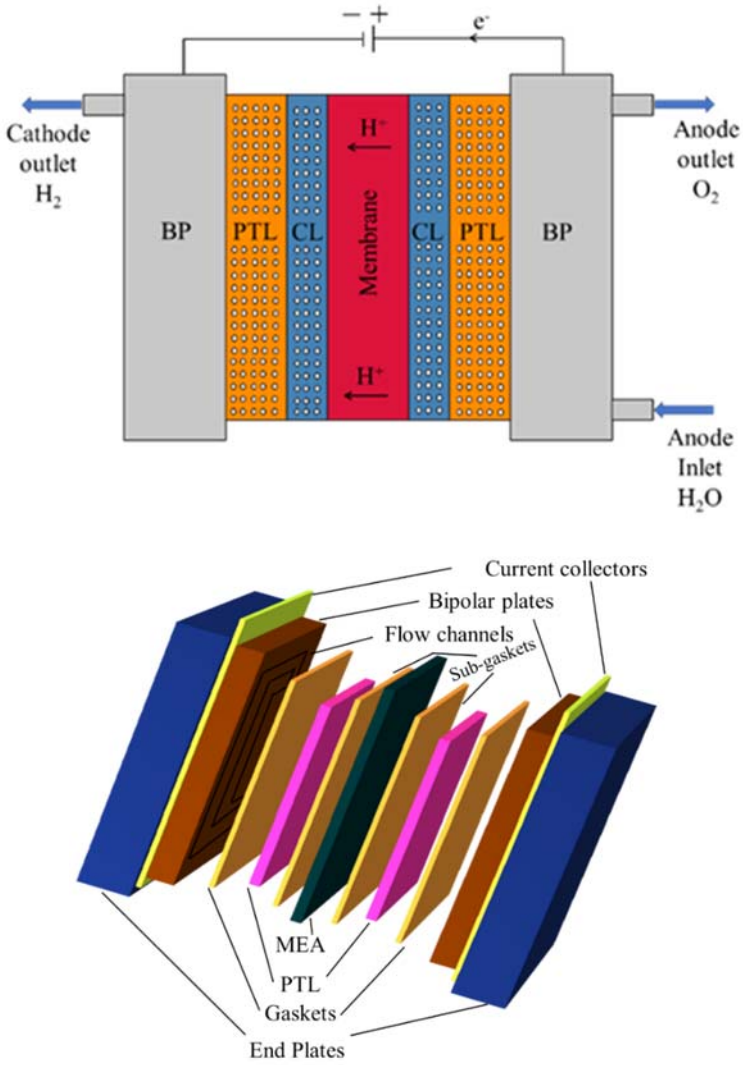

Figure 2. (**Top**): A 2-D schematic of a PEMEC with reactant and product flow. (**Bottom**): A 3-D detailed illustration of a PEMEC with key elements of a PEMEC.

4.1. Membrane Electrode Assembly (MEA) and Key Layers

4.1.1. Membrane

At the centre of a PEMEC is the proton exchange membrane, whose primary function is to facilitate proton (H^+) transport from the anode to the cathode while preventing electron (e^-) crossover. This selective permeability is critical for maintaining efficient electrolysis. Among commercially available membranes, Nafion (a perfluorosulfonic acid, PFSA) is the most widely used due to its high proton conductivity and chemical stability.

The performance of the membrane depends on its hydration level and operating temperature, typically between 50 and 80 °C. At lower hydration levels, proton conductivity

decreases, leading to higher ohmic losses. Conversely, excessive water retention can result in membrane swelling, affecting durability [36,37].

4.1.2. Anode and Cathode Catalyst Layers (CLs)

The CLs, located on either side of the membrane, facilitate the oxygen evolution reaction (OER) at the anode and the hydrogen evolution reaction (HER) at the cathode. Due to the highly oxidative environment at the anode, iridium oxide (IrO_2) and ruthenium-based catalysts are commonly used, whereas platinum (Pt) catalysts are employed at the cathode [18,38].

Typical CL thicknesses range from 12 to 30 μm, and their porosity significantly affects mass transport [15,39]. Higher porosity improves reactant diffusion but may compromise electrical conductivity. Optimizing catalyst layer composition, loading, and porosity remains a major challenge for improving PEMEC performance and reducing costs.

4.1.3. Anode and Cathode PTLs

The PTLs, positioned between the catalyst layers and bipolar plates, play a critical role in PEMEC performance by ensuring efficient reactant transport, gas removal, and electrical connectivity. They facilitate the transport of water to the catalyst layers, allowing continuous electrolysis to occur while simultaneously enabling the removal of generated oxygen and hydrogen gases from the reaction sites. In addition to gas and liquid management, PTLs enhance electrical conductivity by providing a conductive path between the CLs and the BPs, thereby minimizing ohmic losses. Another crucial function of PTLs is thermal regulation, as they help dissipate heat generated during operation, contributing to overall cell stability. PTLs can be made from carbon-based materials or titanium-based materials (especially for the anode side, where oxidative stability is required) [40]. PTL thickness typically ranges between 250 μm and 1.1 mm, depending on the material and operating conditions [15]. In high-temperature PEMECs, where only water vapor is present, a gas diffusion layer (GDL) may replace the PTL, focusing solely on gas transport. The choice between PTL and GDL depends on temperature, phase interaction, and electrolyte management requirements [36,41].

4.2. Structural and Support Components

4.2.1. Gaskets

Gaskets are essential for gas segregation, sealing, and mechanical stability within a PEMEC. In a typical configuration, four gaskets are used: two sub-gaskets between the membrane and PTLs and two additional gaskets between the BPs and PTLs [39,42]. Common gasket materials include perfluoroelastomer (FKM), known for its high chemical resistance and thermal stability, and butyl rubber, which offers excellent gas impermeability. A well-designed gasket ensures minimal gas crossover, preventing recombination losses and preserving efficiency [39,42].

4.2.2. Bipolar Plates (BPs)

Bipolar plates (BPs) facilitate reactant distribution and electron conduction between adjacent cells in a stack. They typically contain flow-field channels that ensure uniform water distribution and gas evacuation [41]. The material selection for BPs is crucial for durability and efficiency. Titanium (Ti) is widely preferred due to its high durability and corrosion resistance, while coated stainless steel (SS) serves as a lower-cost alternative with protective coatings to enhance longevity [43]. In industrial-scale PEMECs, BPs larger than 5 cm × 5 cm are commonly used, incorporating customized flow-field designs to

optimize reactant transport and efficiency [15]. Some advanced designs also include cooling channels to regulate temperature and improve overall system stability [28,44].

4.2.3. Current Collectors

Current collectors ensure efficient electron transport between the bipolar plates and the external circuit. Typically made from stainless steel or other corrosion-resistant alloys, they are sometimes integrated into the bipolar plates to minimize ohmic losses and enhance mechanical stability [45]. Their configuration directly influences ohmic polarization, which in turn impacts overall cell efficiency [45].

4.2.4. End Plates

End plates provide mechanical compression to maintain electrical contact between the PEMEC components. In multi-cell stacks, they prevent performance degradation caused by misalignment or gas leaks [43]. Proper compression ensures uniform contact resistance across the stack, preventing reactant leakage and contributing to extended operational stability [43].

4.3. Performance Enhancement Strategies in PEMECs

High-efficiency operation in PEMECs depends on the optimization of catalysts, membranes, electrode structures, and flow-field configurations. These elements influence key performance parameters such as mass transport, ohmic losses, and overpotentials [35]. While significant progress has been made experimentally, there remains a need for systematic modelling approaches to evaluate and predict the effectiveness and durability of these enhancements under varying operating conditions.

4.3.1. Catalyst Optimization

The catalyst layers (CLs) are central to the oxygen evolution reaction (OER) at the anode and the hydrogen evolution reaction (HER) at the cathode. Although iridium oxide (IrO_2) and platinum (Pt) are widely used for their catalytic activity, their high cost and limited availability hinder scalability [31]. To address this, single-atom catalysts, nanostructured systems, and metal oxide–carbon composites have been developed [46,47]. While these innovations demonstrate improved HER efficiency and catalyst utilization, critical gaps remain in evaluating their long-term stability and performance under real-world conditions. Current modelling efforts often exclude material degradation and morphological evolution, which are vital to accurately assess catalyst durability. Integrating such features into PEMEC models would support more reliable lifecycle predictions and aid in material selection for scale-up. A summary of commonly used catalyst materials and their roles in PEMEC systems is provided in Table 2.

Table 2. Common catalysts used in industries.

Catalyst	Position	Role	Ref
IrO_2	Anode	Facilitate OER	[48,49]
Pt	Cathode	Facilitate HER	[18,38]
Molybdenum (Mo)	Anode	Facilitate HER	[50]
Nickel-Iron (NiFe)	Cathode	Facilitate HER	[51]
Cobalt based (Co)	Cathode	Facilitate HER	[52,53]
Composite Catalysts (Metal Oxides + Carbon)	Cathode	Facilitate HER	[54]
Single-atom catalysts	Cathode	Maximize catalyst efficiency	[46,47]

4.3.2. Membrane Material and Configuration Improvements

The membrane plays a vital role in PEMECs by enabling selective proton transport while preventing gas crossover. Nafion, a perfluorosulfonic acid (PFSA) membrane, remains the most widely adopted due to its high proton conductivity and proven durability [12,19,55,56]. However, its high cost and performance limitations under dry or high-temperature conditions have motivated exploration of alternatives. Materials such as sulfonated polyether ether ketone (SPEEK), polybenzimidazole (PBI), and various polymer blends offer cost-effective options with tuneable properties [20,37,57–61]. Although these alternatives reduce material costs, they often require further enhancements in durability, particularly regarding swelling resistance, chemical degradation, and hydration retention during long-term operation.

Recent efforts have also focused on reducing membrane thickness to lower ohmic resistance. While thinner membranes can improve ionic conductivity and efficiency, they often compromise mechanical stability. To mitigate this trade-off, hybrid membrane designs incorporating inorganic additives (e.g., phosphosilicate glasses or nanoparticles) have been proposed to enhance structural integrity while maintaining high proton conductivity [62]. However, most modelling studies treat membrane properties as static and homogeneous, neglecting critical behaviours such as swelling, thinning, conductivity loss, and mechanical stress under electrochemical loads.

A recent study by Østenstad [63] introduced a multiphysical modelling framework for a next-generation PEM electrolyzer featuring ultra-thin membranes, highlighting how membrane deformation and coupled proton transport significantly affect performance prediction. Such models demonstrate the importance of accounting for transient operating conditions, particularly for high-efficiency operation with a reduced membrane thickness.

A comparative summary of common membrane materials used in PEMECs is provided in Table 3, highlighting their advantages, limitations, and relevance to industry applications.

Table 3. Common membranes used in industries.

Membrane	Features/Pros/Cons	Ref
Nafion (PFSA)	Commercial, high proton conductivity, durable, expensive; widely used in PEM fuel cells and reliable	[20,37,57]
SPEEK	Hydrocarbon-based, cost-effective, good chemical stability	[58,59]
PBI	High temperature resistance, used in acid-alkaline environments	[60,61]
Polyphenylene oxide (PPO)	Aromatic hydrocarbon-based, cost and performance balance	[64,65]
Polymer blends	Optimized mix for conductivity, strength, and stability	[66]
Inorganic-organic hybrid	Embedded nanomaterials for improved stability, still under investigation	[67,68]
Anion exchange membrane	Anion exchange instead of cation exchange, used in both alkaline and PEM, conductive of negatively charged ions, low alkaline stability	[69–71]

Improved multiphysics models that couple proton transport, water content, and mechanical deformation are needed to more accurately assess membrane performance under dynamic and long-term operation. Such models would enable more predictive design and better evaluation of emerging materials [62].

4.3.3. Innovative Electrode Designs

Optimizing electrode architecture is essential for enhancing mass transport, catalytic activity, and uniform reactant distribution in PEMECs. Electrodes typically consist of catalyst layers (CLs) supported on porous substrates, where the hydrogen evolution reaction (HER) occurs at the cathode and the oxygen evolution reaction (OER) at the anode [72,73]. Novel designs aim to address key performance bottlenecks, including gas-liquid transport

and water management [48]. While various solutions have been proposed [3,4,12,55,74], many remain insufficiently modelled, particularly under dynamic or transient operating conditions.

a. Gas Diffusion Electrodes (GDEs)

GDEs form a tri-phase interface (solid-liquid-gas) that enhances electrochemical kinetics and is widely used at both electrodes. Cathodes typically employ carbon-based substrates like carbon paper or cloth for their porosity and conductivity, while the anode, exposed to harsh oxidative conditions, uses titanium-based GDEs for corrosion resistance [62,75]. Despite their widespread use, most modelling studies treat GDEs as homogenous layers, ignoring pore-scale variations, potential gradients, or localized flooding. Incorporating porous structure, compression effects, and saturation dynamics into models would provide a more realistic evaluation of long-term GDE performance.

b. Flow-Field Design

Flow-field architecture in bipolar plates plays a key role in distributing reactants and removing gaseous products. These channels affect mass transport resistance and pressure drop across the electrode surface [26]. Common flow-field geometries—parallel, serpentine, spiral, and interdigitated—offer varying degrees of reactant uniformity, pressure control, and gas evacuation [76]. Each configuration involves trade-offs between performance and energy efficiency, which are often evaluated experimentally but rarely through comprehensive modelling approaches.

For instance, parallel designs minimize pressure drop but can suffer from uneven gas removal, while serpentine and interdigitated patterns improve gas–liquid interaction at the cost of higher-pressure losses [77,78]. Spiral configurations are more compact and suited to circular cells but require careful optimization to avoid flow stagnation. These variations, illustrated in Figure 3, underscore the importance of geometry on electrochemical performance [14]. Despite their influence on PEMEC efficiency, most modelling studies simplify flow-field effects using idealized or 2D approximations, ignoring spatial gradients and multiphase dynamics. With the growing availability of 3D printing for precise flow-field fabrication [21], it is increasingly feasible—and necessary—to incorporate real flow-field geometries into computational models. Doing so would enable predictive simulations of pressure profiles, reactant utilization, and localized degradation phenomena under realistic operating conditions.

Tofighi-Milani et al. [79] further emphasized the need for dynamic modelling frameworks that capture electrical and flow-related transients within electrolyzer architectures. Their work pointed out that while flow-field designs are well-characterized experimentally, most models fail to capture system-level behaviours under load cycling, which is crucial for integration with renewable sources.

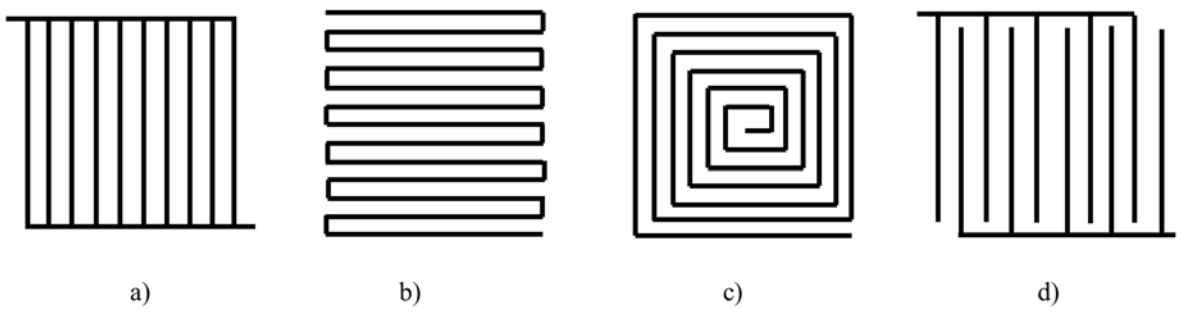

Figure 3. Most common flow-field designs in the PEMEC. (**a**) Parallel, (**b**) serpentine, (**c**) spiral, and (**d**) interdigitated.

c. Porous Electrode Substrates

Porous substrates provide mechanical support and enable gas diffusion in the catalyst layers of PEMECs. Carbon-based materials such as carbon paper and carbon cloth are widely used at the cathode for their electrical conductivity, porosity, and stability under reducing conditions [80]. However, at the anode, carbon substrates degrade rapidly due to oxidative and acidic environments, making titanium (Ti)-based substrates the preferred option for long-term durability [12,81,82]. Titanium substrates exhibit excellent corrosion resistance, high electrical conductivity, and strong mechanical integrity, which are essential for sustaining stable PEMEC performance. Yet, despite their critical role, their microstructural effects on multiphase transport and electrochemical performance are often oversimplified or omitted in numerical models. Incorporating realistic porosity gradients, mechanical stress, and contact resistance into simulations could improve predictions of electrode performance and aging over time. This is especially important under dynamic operating conditions, where phase saturation and structural compression may evolve nonlinearly.

In this context, Østenstad [63] proposed a modelling approach that resolves localized saturation and electrochemical activity through the porous anode structure, demonstrating that even minor variations in porosity and layer thickness lead to measurable shifts in reaction zones and gas transport efficiency.

d. Three-Layer Electrodes

The integration of a catalyst layer, microporous layer (MPL), and gas diffusion layer (GDL) into a three-layer electrode design has emerged as a promising strategy for improving PEMEC efficiency. Each layer performs a distinct function: the MPL facilitates water management by preventing flooding or drying, while the GDL ensures efficient gas transport and reactant delivery [12,28].

While the functional synergy of these layers is well established experimentally, modelling their combined behaviour remains limited. Most numerical approaches treat electrodes as single, homogenous domains, overlooking interfacial effects, pore size distribution, and coupled capillary dynamics. Emerging designs, such as nanostructured electrodes, carbon nanotube-enhanced supports, and 3D-printed electrode architectures, introduce even more complexity in terms of structure and material interactions [83,84]. To evaluate these innovations systematically, multiscale or pore-network modelling techniques are required, particularly for analyzing the impact of geometry on water retention, gas evolution, and mechanical reliability.

Recent reviews such as Tofighi-Milani et al. [79] stress the importance of integrating electrical dynamics with layered electrode behaviour to predict transient responses, highlighting that multiscale modelling is essential for bridging the gap between component-level design and system-level control.

5. Research Gap

Based on our literature review, it is evident that while PEM electrolyzers achieve slightly higher efficiencies (70–80%) compared to their alkaline counterparts (65–75%), their widespread adoption is hindered by high costs. This is primarily due to the reliance on iridium—a scarce and expensive catalyst—and the extensive use of costly materials in their construction. Additionally, both PEM and AWE are limited by low operating temperatures, which further constrains their efficiency. The challenges associated with PEM electrolyzers range from material costs to durability concerns.

Table 4 summarizes the primary challenges affecting PEM electrolyzers, including material costs, durability, and operational limitations, along with research strategies aimed at mitigating these issues through material innovation and numerical modelling. These research directions indicate the growing role of numerical modelling and material

innovation in overcoming the limitations of PEM electrolyzers. To address these challenges, advanced numerical modelling has become an essential tool for optimizing catalyst utilization and improving material selection. Computational methods such as density functional theory (DFT) and molecular dynamics (MD) enable atomic-level investigations of reaction mechanisms, facilitating the identification of alternative catalyst materials with desirable properties [85,86]. High-throughput screening techniques significantly reduce the reliance on costly and time-intensive experimental trials, accelerating the discovery of cost-effective and sustainable alternatives to iridium-based catalysts. Furthermore, numerical models provide insights into catalyst distribution and utilization within electrode layers, minimizing material requirements while maintaining performance. These simulations also offer predictive guidance for experimentalists, allowing targeted validation of promising materials and ensuring a more efficient research and development process [87]. Despite their advantages, PEM electrolyzers still face durability challenges, particularly in maintaining performance over long operational lifetimes. For industrial applications, PEM systems are expected to operate for 40,000 to 60,000 h [12]. However, consistently achieving these benchmarks remains difficult due to catalyst degradation, membrane thinning, mechanical stress, and contamination from impurities. The exposure of PEM components to harsh chemical environments accelerates corrosion, reducing their lifespan. Additionally, variations in operating conditions—such as temperature fluctuations and high-current densities—exacerbate mechanical stress and potential failures [12]. Durability remains a major challenge for PEM electrolyzers due to multiple degradation mechanisms that impact key components. Figure 4 presents the major degradation mechanisms affecting PEM electrolyzers, highlighting the contributions of catalyst degradation, membrane thinning, and other key failure modes. As seen in Figure 4, catalyst degradation and membrane thinning account for the largest share of failure mechanisms, underscoring the need for innovative material solutions and optimized operating conditions to improve long-term performance. Numerical modelling plays a crucial role in addressing these durability challenges by simulating key degradation mechanisms such as catalyst sintering and dissolution, membrane thinning due to chemical attack, and mechanical stresses in PTLs and catalyst layers (CLs). These simulations quantify the impact of operating conditions—including temperature, humidity, and current density—on system longevity [88]. Lifetime prediction models integrate degradation rates into performance simulations, allowing researchers to forecast long-term stability and optimize component designs accordingly. Additionally, flow-field and porous layer optimizations—enabled by numerical studies—help mitigate mechanical stress and improve durability by ensuring uniform reactant distribution. Many of these models are validated against long-term experimental data, reinforcing their accuracy and reliability [89].

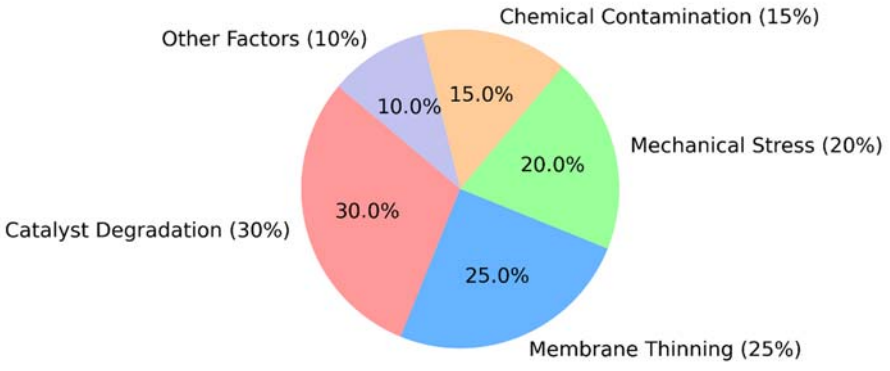

Figure 4. Major degradation mechanisms in PEM electrolyzers [39,90].

Table 4. Key challenges and research directions for PEM electrolyzers.

	Challenges	Current Limitations	Research Direction
1	High material cost	Expensive iridium-based catalysts	Development of alternative catalyst
2	Durability issues	Shorter operational lifespan	Enhancing durability through structural improvements
3	Limited operating temperature	Efficiency constraints due to temperature	Optimizing thermal management
4	Catalyst degradation	Iridium dissolution, sintering effects	Modelling and mitigating degradation mechanisms
5	Membrane thinning	Chemical degradation, mechanical wear	New membrane materials with improved stability
6	Complex electrochemical reactions	Computational complexity	Developing computationally efficient models
7	Two-phase flow modelling	Difficult to simulate accurately	Advanced two-phase flow simulation for better accuracy

A deeper understanding of PEM electrolyzer performance is essential for optimizing operating conditions and ensuring long-term stability. While numerical and experimental studies provide valuable insights into degradation rates and system weaknesses, replacing costly and time-intensive experimental setups with accurate simulations remains a significant challenge, particularly when modelling complex phenomena such as two-phase flows and intricate electrochemical reactions [15]. There is a pressing need for computationally efficient yet accurate models that balance predictive power with practical implementation. Additionally, integrating fast-response control systems capable of adapting to dynamic operating conditions will be crucial for advancing this technology. By addressing these challenges, future research can further enhance the economic viability, durability, and overall performance of PEM electrolyzers.

6. Mathematical Modelling and Simulation

Modelling and simulation play a crucial role in understanding the complex electrochemical and transport processes in proton exchange membrane electrolyzer cells (PEMECs). Numerical simulation models provide detailed insights into system behaviour, helping to optimize design and operating conditions. Over the years, various models—ranging from zero-dimensional analytical models to three-dimensional CFD simulations—have been developed to quantify the key physical and electrochemical phenomena occurring in PEMECs. This section presents the governing equations, boundary conditions, and initial conditions used in these models, along with a comparison of their assumptions and predictive capabilities. A particular focus is placed on the differences between single-phase and multi-phase models, which play a crucial role in capturing gas evolution and water transport mechanisms. In addition, emerging methodologies such as multi-scale modelling, computational fluid dynamics (CFD), and machine learning (ML)-based optimizations are discussed [14,16,27,78,91,92]. Table 5 summarizes various modelling approaches for PEMEC simulations, categorizing them based on their complexity and the physical aspects they incorporate.

i. Zero-dimensional model

Choi et al. [17] developed a zero-dimensional model to analyze PEM electrolysis cells based on steady-state mass balances and electrochemical kinetics. The net molar production or consumption rates of water, hydrogen, and oxygen are governed by Faraday's law, expressed in differential form as:

$$\begin{cases} \frac{dN_{H_2O}}{dt} = -\frac{iA}{2F} \\ \frac{dN_{H_2}}{dt} = \frac{iA}{2F} \\ \frac{dN_{O_2}}{dt} = \frac{iA}{4F} \end{cases} \quad (4)$$

where $\frac{dN_j}{dt}$ is the molar production or consumption rate of species j [mole/s], i is local current density [A/m²], A is the active electrode area [m²], and F is Faraday's constant [C/mole]. These flow rates are directly related to the electrochemical reactions governed by the cell potential. Under the assumption of no mass transport limitations, the current density can be linked to the cell overpotential (η) using a simplified form of the Butler–Volmer equation, as stated below [93]:

$$i = i_{a0}\left[exp\left(\frac{F\eta_a\,\alpha_a\omega_{e^-}}{RT}\right) - \exp\left(\frac{F\eta_a(\alpha_a - 1)\omega_{e^-}}{RT}\right)\right] \quad (5)$$

where i_{a0} represents the anode exchange current density (under the well-mixed condition at the anode). η_a is the overpotential at the anode chamber that can be expressed as a function of temperature (T), current density (i), and anode exchange current density (i_{a0}), alternatively. ω_{e^-} and α_a are the stoichiometric coefficient for electrons in the anode and transfer coefficient which have the values of 2 and 0.5, respectively [94]. Assuming these values, the anode overpotential can be expressed explicitly as Equation (6).

$$\eta_a = \frac{RT}{F}\sinh^{-1}\left(\frac{i}{2\,i_{a0}}\right) \quad (6)$$

The overpotential can be written in the form of cathode parameters (i_{c0}, η_c, and α_c) where ω_{e^-} and α_c take values of −2 and 0.5, respectively (Equation (7)).

$$\eta_c = -\frac{RT}{F}\sinh^{-1}\left(\frac{i}{2\,i_{c0}}\right) \quad (7)$$

To simulate the membrane potential (φ), the divergence of current density is considered to be zero along with the steady-state conditions (no change over time). Consequently, the current density becomes directly proportional to the membrane potential, with electrolyte conductivity (σ) serving as the factor equalizing this proportionality (Equation (8)).

$$i = -\sigma\,\nabla\varphi \quad (8)$$

Considering all available potential sources, e.g., Nernst potential, anode, cathode, and membrane overpotentials and losses in an electrolysis cell (see [17]), an expression can be employed to determine the overall voltage (V) in relation to the current density (i). This relationship (Equation (9)) yields a polarization plot.

$$V = V_0 + \frac{RT}{F}sinh^{-1}\left(\frac{i}{2\,i_{a0}}\right) + \frac{RT}{F}sinh^{-1}\left(\frac{i}{2\,i_{c0}}\right) + \frac{L_M}{\sigma_M}\,i + ri \quad (9)$$

where V_0, L_M, σ_M, and r are the Nernst potential, membrane thickness, membrane conductivity, and interfacial resistance, respectively. In the work of [17], this curve was plotted and compared with the experimental findings in [95]. However, their model did not consider heat transfer and lacked porous membrane simulations, limiting its accuracy [17]. In PEM modelling (both PEMFC and PEMEC), the term "single-phase" refers to water existing solely in liquid or vapor form within the system, whereas multi-phase models incorporate gas bubble formation and liquid–gas interactions.

Table 5. Evolution of numerical modelling for PEMEC—from simplified to advanced approaches.

Model	Study Description	Key Output	Ref
0D models	Simplified electrochemical kinetics in PEMEC with no heat and mass transfer considerations.	Analyzed overpotentials across a range of current densities.	[20]
	Heat transfer and fluid flow simulation in PEMEC without electrochemical kinetics or liquid–gas interaction.	Investigated pressure drop in bipolar plates numerically and experimentally.	[80]
	Gas–fluid flow simulation in PEMEC with no electrochemical kinetics.	Presented velocity and pressure contours and compared results with single-phase flow data.	[95]
Single-phase 3D models	Heat and mass transport modelling in PEMEC with simple electrochemical kinetics (no gas–liquid interaction).	Hydrogen generation in high-temperature PEMEC analyzed through polarization curves.	[23]
	Comprehensive PEMEC model incorporating detailed electrochemical kinetics (no gas–liquid interaction).	Examined polarization curves at different temperatures and analyzed the effect of exchange current density.	[96]
	PEMEC modelling with multiple fluid flow configurations (no gas–liquid interaction).	Investigated the effect of different flow configurations on polarization performance.	[24]
Two-phase 3D models	PEMEC modelling under low-temperature conditions with detailed electrochemical kinetics.	Conducted an analytical study of PEMEC behaviour under low- and high-potential conditions.	[15]
	Non-isothermal, transient PEMEC model.	Studied temperature stabilization under various operational conditions.	[97]
	PEMEC simulation including gas–liquid interactions, integrated with electrochemical kinetics.	PEMEC simulation including gas–liquid interactions, integrated with electrochemical kinetics.	[14]

ii. Single-phase model

In 2009, Nie et al. [78] performed a three-dimensional numerical simulation to assess the fluid flow in the bipolar plates of a PEMEC using a single-phase model. The principles and governing equations in a PEMEC are very similar to the those in the work of Ubong et al. [41] for a PEM fuel cell (PEMFC) operating at elevated temperatures with some minor distinctions. The objective of a PEMEC is to generate hydrogen from water with the aid of an external voltage, while in the PEMFC, hydrogen is used as fuel water to generate voltage. The membrane in the PEMFC is still used to separate the anode and cathode compartments and allows for the transport of protons (H^+) from the anode to the cathode but in reverse. Hydrogen is typically fed into the anode, and oxygen (or air) is fed into the cathode. At the anode, hydrogen is oxidized, producing protons and electrons. The protons migrate through the PEM to the cathode, where they combine with oxygen and electrons to form water. The flow of electrons through an external circuit generates electric power [41,72,73]. The electrochemical reactions in a PEMFC are shown in Equation (10).

$$\begin{aligned} 2H_2 &\rightarrow 4H^+ + 4e^- \quad \text{Anode} \\ O_2 + 4H^+ + 4e^- &\rightarrow 2H_2O \quad \text{Cathode} \\ 2H_2 + O_2 &\rightarrow 2H_2O \quad \text{Overall} \end{aligned} \tag{10}$$

The mass conservation equation in a single-phase flow within homogeneous and isotropic porous media (PEM elements, e.g., membrane, PTL, CL) can be expressed in a general form as Equation (11) [26].

$$\nabla.(\rho\varepsilon\tilde{u}) = S_m \tag{11}$$

where $\tilde{u}$, ρ, and ε are the velocity vector, density, and porosity, respectively. S_m represent the source term accounting for the generation or consumption of mass within the system. The momentum equations for the single-phase flow in porous media can be written in the form of Equation (12) [98].

$$\nabla.(\rho\varepsilon\tilde{u}\tilde{u}) = -\varepsilon\,\nabla p + \nabla.(\varepsilon\,\tilde{\tau}) + S_u \tag{12}$$

where p and S_u represent pressure and the source term in momentum equations, respectively. τ represents the tension tensor, which in Newtonian fluid can be expressed in terms of the velocity gradient (Equation (13)) [26].

$$\tau = \mu\,[\nabla\tilde{u} + (\nabla\tilde{u})^T] \tag{13}$$

where μ represents the dynamic viscosity of the gas.

Within porous media, Darcy's law can be applied to relate the pressure drop to the gas velocity. The source term in Equation (12) can be expressed as Equation (14) [77]:

$$S_{\boldsymbol{u}} = -\frac{\mu}{K}\varepsilon^2\tilde{u} \tag{14}$$

where K and ε are the permeability and porosity of porous media, respectively. Permeability can be determined using the Kozeny – Carman model [26]:

$$K = \frac{d_P^2}{180}\frac{\varepsilon^3}{(1-\varepsilon)^2} \tag{15}$$

where d_P represent the particle diameter of porous material. The value of these two parameters may vary in different materials and across different sections in the PEMEC (See Table 6).

Beyond porosity and permeability, tortuosity (tor) significantly influences effective transport properties in porous electrodes by accounting for the complexity of internal pore paths. Similarly, electrical conductivity governs charge transport in PTLs and CLs and must be accurately represented in multiphysics models to predict electrochemical performance.

Table 6. Porosity and permeability of PEM elements.

Property	Symbol	Value/Range	Ref
Membrane porosity	ε_M	0.4–0.6	[77]
PTL porosity	ε_{PTL}	0.2–0.6	[77]
CL porosity	ε_{CL}	0.3–0.5	[77]
Membrane permeability	K_M	10^{-10}–10^{-8} (m²)	[77]
PTL permeability	K_{PTL}	10^{-13}–5×10^{-12} (m²)	[41]
CL permeability	K_{CL}	10^{-16}–5×10^{-14} (m²)	[41]
PTL tortuosity	$tor_{\,PTL}$	2–4	[41]
CL tortuosity	tor_{CL}	1.5–3	[41]
PTL conductivity	σ_{PTL}	1000–20,000 S/m	[41]
CL conductivity	σ_{PTL}	100–1000 S/m	[41]

The molar concentrations of the active species in the process of electrolysis (hydrogen, oxygen, and water) are determined by solving the conservation of species (Equation (16)) [77].

$$\nabla.\left(\varepsilon\tilde{u}\,C_j\right) = \nabla.(D_j^{eff}\,\nabla C_{\,j}) + S_j \tag{16}$$

where C_j and D_j^{eff} are molar concentration and effective diffusion coefficient of each species. D_j^{eff} is the function of cell operating conditions like temperature and pressure and can be expressed as Equation (17) [77].

$$D_j^{eff} = \varepsilon^{3/2} D_j^0 \left(\frac{T}{T_0}\right)^{3/2} \left(\frac{p^0}{p}\right) \tag{17}$$

where T_0 and P_0 denote the reference temperature and pressure. D_j^0 is the reference diffusivity of hydrogen, oxygen, and water, which are 1.1 × 10^{-4}, 3.2 × 10^{-5}, and 7.35 × 10^{-5} ($m^2 s^{-1}$), respectively [77,91]. S_j refers to the source term for each species and can be expressed as Equation (18) [96]:

$$\begin{aligned} S_{H_2O} &= -\frac{i_a M_{H_2O}}{2F} \\ S_{H_2} &= \frac{i_c M_{H_2}}{2F} \\ S_{O_2} &= \frac{i_a M_{O_2}}{4F} \end{aligned} \tag{18}$$

where M is the molecular weight of the species, which has the value of 18, 2, and 32 [gr/mole] for water, hydrogen, and oxygen, respectively.

In steady-state conditions, there is a simple balance between proton current in the membrane (i_l) and electron current in the electrodes (i_s), which is stated in Equation (19) [93].

$$\nabla . i_l + \nabla . i_s = 0 \tag{19}$$

where i_l and i_s can be calculated by Ohm's law [93].

The next important governing equations used to determine the proton and electron potential and are expressed as Equations (20) and (21) [77]

$$\nabla . \left(\sigma_e^{eff} \nabla \varphi_e\right) + S_{\varphi_e} = 0 \tag{20}$$

$$\nabla . \left(\sigma_s^{eff} \nabla \varphi_s\right) + S_{\varphi_s} = 0 \tag{21}$$

where φ_e and σ_e^{eff} are the membrane (electrolyte) electrical potential and effective ion conductivity, respectively, while φ_s and σ_s^{eff} are corresponding parameters in the solid phase (electrode). S_{φ_e} and S_{φ_s} are the source terms for the protonic and electrical potentials, respectively, which can be simply related to the current density (i), as shown in Equation (22) [41,77].

$$S_{\varphi_e} = S_{\varphi_s} = i \tag{22}$$

The effective electronic and membrane conductivities can be estimated using Bruggeman's approach, which serves as a reliable approximation [97]. As the effective membrane conductivity is also a function of temperature (T) and humidification degree in the membrane (λ), the following expression can be used for it [96,99].

$$\sigma_e^{eff} = 100\, \varepsilon^{3/2} \times \exp\left[1268 \left(\frac{1}{303} - \frac{1}{T}\right)\right] \times (0.005139\lambda - 0.00326) \tag{23}$$

The last governing equation that determines the temperature distribution within the PEM cell is the energy equation in porous media. It can be expressed as Equation (24) [100].

$$\nabla . (\rho \varepsilon\, C_P \tilde{u} T) = \nabla . (k^{eff} \nabla T) + S_e \tag{24}$$

where C_P and k^{eff} are specific heat at constant pressure and effective thermal conductivity.

There are various models to calculate the effective thermal conductivity, the most important of which are parallel, series, and geometric. One of the easiest models is using the parallel model, in which the fluid and the solid are parallel to the heat flow. It is a linear correlation, as shown below [101]:

$$k^{eff} = (1-\varepsilon)k_s + \varepsilon\, k_f \quad (25)$$

where k_s and k_f are the thermal conductivity of a solid (catalyst electrode) and liquid electrolyte (membrane), respectively. In this model, heat flows independently through the liquid and solid. In the series model, heat passes through each layer in sequence. Using a series model produces the lowest value for effective thermal conductivity [101]. A brief comparison between the calculated amount of effective thermal conductivity using various methods is presented in Table 7.

Table 7. Effective thermal conductivity using $k_s = 1\ \mathrm{Wm^{-1}K^{-1}},\ k_f = k_s/5,\ \varepsilon = 0.4$.

Model	Formulation	Value
Parallel [100]	$k^{eff} = (1-\varepsilon)k_s + \varepsilon\, k_f$	0.68
Series [100]	$k^{eff} = \left[(1-\varepsilon)/k_s + \varepsilon/k_f\right]^{-1}$	0.38
Geometry [100]	$k^{eff} = {k_s}^{(1-\varepsilon)} + {k_f}^{\varepsilon}$	0.525
Modified Maxwell [101]	$k^{eff} = \left(\frac{1-\varepsilon}{3k_s} + \frac{\varepsilon}{2k_s+k_f}\right)^{-1} - 2k_s$	0.62

The source term in the energy equation (S_e) may vary across different sections (e.g., anode CL, cathode CL, solid phase, and membrane). Neglecting the heat sources produced by irreversible reactions and entropic heat generation because of the reactions (in anode and cathode CL), the source term for different elements in a PEM can be simplified as shown in Table 8 [89].

Table 8. Energy source term in Equation (24) produced by electrochemical reactions [89].

Element	Formulation for Source Term	Unit
Membrane	$(S_e)_M = \sigma_e^{eff}\,(\nabla\varphi_e)^2$	W m^{-3}
Solid phase	$(S_e)_S = \sigma_s^{eff}\,(\nabla\varphi_s)^2$	W m^{-3}
Anode CL	$(S_e)_{An} \approx (S_e)_S + (S_e)_M$	W m^{-3}
Cathode CL	$(S_e)_{Ca} \approx (S_e)_S + (S_e)_M$	W m^{-3}

Ruiz et al. [102] developed a three-dimensional mathematical model to investigate key electrochemical and thermal phenomena in high-temperature PEMECs (above 100 °C). Their study highlighted several advantages of operating at elevated temperatures, including enhanced electrode kinetics, reduced overpotentials, lower thermodynamic energy requirements, and a decrease in reversible voltage. Additionally, the model incorporated a more detailed heat and mass transfer analysis in conjunction with electrochemical kinetics [102].

That study further examined the impact of three different flow channel configurations—parallel, serpentine, and multi-serpentine—on hydrogen production and temperature distribution. Using a single-domain model in ANSYS Fluent 13 with non-isothermal flow properties, their results showed that the multi-serpentine design offered superior performance by promoting a more uniform temperature distribution. Notably, the model assumed a single-phase flow, neglecting the presence of liquid water due to the elevated operating temperature.

As discussed in the preceding section, the design of the flow field significantly impacts cell performance [48]. Toghyani et al.'s [77] study illustrated that altering the arrangement of the flow field led to changes in the distribution of reactants and products transferring toward the PEMEC outlet. The researchers employed a 3D model to simulate the electrolyte in three different arrangements: a parallel flow field (with and without metal foam as a flow distributor), a double serpentine flow field, and a simple channel filled with metal foam. The most recent arrangement exhibited superior performance in

hydrogen production, temperature distribution, current density, and pressure drop [77]. According to their findings, reducing the permeability of the porous media results in an increased pressure drop in the system and enhanced performance of the electrolyzers. Consequently, the optimal permeability for the foam should be carefully selected. In terms of porosity, they modelled this property as a macro-scale feature rather than a micro-structural one. They adopted a single-phase, non-isothermal, and steady-state assumption to streamline their 3D numerical simulation using the finite volume method. Additionally, they illustrated that the spiral flow field leads to greater uniformity in hydrogen distribution [77,91]. A schematic correlation between the relevant physics and parameters involved in analyzing a PEMEC (either in single-phase or multi-phase flow) is illustrated in Figure 5.

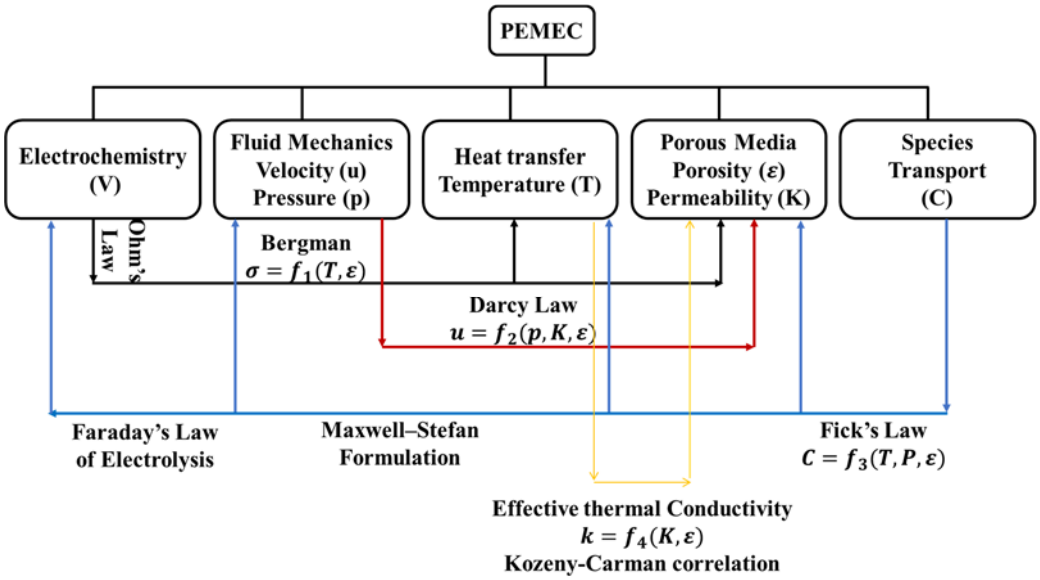

Figure 5. Schematic illustration of physics and parameters correlation in PEMEC analysis.

iii. Two-phase model

Single-phase mass transport is not a realistic assumption in most PEMEC situations due to the limitations of the model [26]. Numerous researchers have endeavoured to develop comprehensive models aiming to furnish precise insights into critical parameters within PEMEC, such as current density, volume fraction, temperature, and flow velocity. These models should possess the capability to analyze PEMEC not only under high operating temperatures and low-current densities, where single-phase models suffice, but also under low-temperature conditions with high-current densities, where single-phase models fail to deliver accurate data [26,27,41,77,91]. Zinser et al. [103] introduced a two-phase model to account for the transportation of oxygen and water within the anodic PTL in a PEMEC (1D half-cell model). The crucial drying-out process, which significantly influences water management in both PEMEC and PEMFC [28], was investigated in the PTL using pressure distribution and saturation plots. To enhance transport behaviour, a suitable range of macro-structural features, including porosity, permeability, and geometrical features, was identified. This observation aligns with the findings of Kalinnikov et al. [30], who, while considering the limitations of two-phase mass transport in the PTL for different regimes, noted similar improvements [30]. One of the key aspects of studying two-phase mass transport is identifying the critical current density profile and distinguishing the stable regime (with a steady-state profile) from the unstable one (characterized by drying-out) [30,103]. Integrating an electrochemical model that includes simulations of coupled thermal-fluid dynamics, species transport, and electrochemistry into a two-phase

flow provided a more comprehensive understanding of species transport and accurate predictions of overall cell performance [15]. These insights directly aid in optimizing PEMEC stack design by improving PTL structures, catalyst layer configurations, and flow-field geometries to enhance reactant distribution and minimize performance losses.

In 2023, several researchers dedicated their efforts to 3D modelling of PEMEC, aiming to explore the influence of various operational factors such as current densities and temperature on overall PEMEC performance. They also investigated the impact of flow-field configurations on mass transport [14,16,26,27]. A common thread in these studies involved incorporating more sophisticated mass transport considerations into the two-phase flow (comprising water and gas) and conducting numerical simulations using commercial software such as ANSYS Fluent and COMSOL Multiphysics. These simulations varied boundary conditions and initial conditions across different geometries of the PTL and channel arrangements. This approach enabled the analysis of the bubble detachment process during different stages of hydrogen production, including the initial phase, instability, deformation, and separation. Factors such as gravity, buoyancy, and surface tension in the microchannel were considered during this analysis [27]. Additionally, researchers explored gas bubble accumulation on the catalyst using integrated mass transport combined with a classic model. Gas bubble accumulation at the CL reduces effective reactant transport, leading to localized starvation, increased ohmic losses, and uneven current density distribution. Optimized PTL structures and improved two-phase flow management can mitigate these losses, enhancing overall PEMEC performance. An example of this is Jiang et al.'s work [26], where the study revealed that gas discharge could be enhanced by using a combination of PTL and CL to reduce heat and mass loss.

In almost all of the two-phase model simulations, the electrochemical model that was used was the Butler–Volmer equation, which was elaboratively described in previous sections. To simulate two-phase systems, various methods have been employed in different studies. The two most significant models are the mixture model (homogeneous equilibrium) [14,15] and the Eulerian model [26]. While the Eulerian model solves separate continuity and momentum equations for each phase, offering detailed phase tracking, it requires significantly higher computational resources. In contrast, the mixture model assumes local equilibrium and treats the two phases as a single homogeneous medium, reducing computational cost at the expense of phase separation accuracy. The choice between these models depends on the required resolution of gas–liquid interactions and available computational power.

Various methods are available for simulating flow properties within the governing equations. For instance, the Darcy model is utilized to simulate porous media [30,103]. Additionally, the volume of fluid (VOF) model, applicable to both single-phase and multiphase flows, is employed to study phenomena such as bubble growth [104]. The choice of model relies on parameters such as the nature of the flow (e.g., bubbly, annular) and computational sources. The governing equations for these models are described in the following section. Most two-phase PEMEC models assume a bubbly or slug flow regime in the PTL, with gas bubbles forming due to electrochemical reactions. In Eulerian models, phase interactions such as surface tension, drag force, and capillary effects are explicitly included, whereas mixture models assume local phase equilibrium. Typical boundary conditions include constant pressure at the outlet, velocity inlets for water feed, and no-slip conditions at solid interfaces. These assumptions influence the accuracy and computational cost of the simulations and should be selected based on the specific PEMEC operating conditions [14,15].

- Euler model

In this model, separate continuity equations are solved for each phase (liquid and gas), assuming no water evaporation. This implies that the rate of mass transfer between

the two phases is considered negligible [26]. A dimensionless quantity known as volume fraction (f) is defined to determine the relative number of different phases within the flow, which is shown in Equations (26) and (27) [26]:

$$f_l = \frac{V_l}{V_l + V_g} \tag{26}$$

$$f_g = \frac{V_g}{V_l + V_g} \tag{27}$$

where f_l and f_g are liquid and gas volume fractions, respectively. It can be easily concluded that $f_l + f_g = 1$. Thus, the continuity equations for liquid and gas in the flow are Equations (28) and (29), respectively [105].

$$\nabla.(\rho_l f_l \varepsilon\, \tilde{u}_l) = S_l \tag{28}$$

$$\nabla.\left(\rho_g f_g \varepsilon\, \tilde{u}_g\right) = S_g \tag{29}$$

S_l, S_g represent the source terms arising from electrochemical reactions for the active species. These values resemble those in the single-phase model (Equation (18)). Considering the mass change rate between liquid and dissolved water (S_{wd}) within the anode catalysts, the source term associated with water consumption undergoes a slight modification, as expressed in Equation (30) [26].

$$S_l = S_{H_2O} - S_{wd} = -\frac{i_a M_{H_2O}}{2F} - S_{wd} \tag{30}$$

Similar to the single-phase model, the momentum conservation equation in the Eulerian two-phase model can be developed as Equations (31) and (32).

$$\nabla.(\rho_l f_l \varepsilon\, \tilde{u}_l \tilde{u}_l) = -\varepsilon f_l\, \nabla p_l + \nabla.(\varepsilon\, \tilde{\tau}_l) + S_{u_l} \tag{31}$$

$$\nabla.(\rho_g f_g \varepsilon\, \tilde{u}_g \tilde{u}_g) = -\varepsilon f_g\, \nabla p_g + \nabla.(\varepsilon\, \tilde{\tau}_g) + S_{u_g} \tag{32}$$

where $\tilde{\tau}_l$ and $\tilde{\tau}_g$ are tension tensors for liquid and gas, which in Newtonian fluid can be expressed in terms of velocity gradient (Equations (33) and (34)) [106].

$$\tilde{\tau}_l = \mu_l f_l\, [\nabla \tilde{u}_l + (\nabla \tilde{u}_l)^T] \tag{33}$$

$$\tilde{\tau}_g = \mu_g f_g\, [\nabla \tilde{u}_g + (\nabla \tilde{u}_g)^T] \tag{34}$$

The terms μ_l and μ_g denote the dynamic viscosity of the liquid and gas (Pa·s). S_{u_l} and S_{u_g} represent the source terms for the liquid and gas phases. In the context of PEMECs, these terms originate from two distinct sources: (i) viscous resistance between porous walls and fluid and (ii) interaction drag force between liquid and gas [106]. An effective model proposed by Schiller and Naumann is employed to simulate these interactions within various elements of a PEMEC, such as channels, PTL, and catalyst layers, as comprehensively described in [26].

Similar to mass and momentum conservation equations, a set of energy equations can be used to determine the temperature distribution for both gas and liquid phases in PEMECs, as outlined in Equations (35) and (36) [26,107].

$$\nabla.(\rho_l f_l \varepsilon\, C_P \tilde{u}_l T) = \varepsilon \tilde{\tau}_l : \nabla \tilde{u}_l - \nabla.(f_l\, k^{eff}\, \nabla T_l) + f_l \varepsilon\, S_e \tag{35}$$

$$\nabla.\left(\rho_g f_g \varepsilon\, C_P \tilde{u}_g T\right) = \varepsilon \tilde{\tau}_g : \nabla \tilde{u}_g - \nabla.(f_g\, k^{eff}\, \nabla T_g) + f_g \varepsilon\, S_e \tag{36}$$

where S_e represent the energy that is released due to the electrolysis of water and varies throughout different sections within a PEMEC. The main parameters involved in determining the value of S_e are current density (i), membrane conductivity (φ_e), and solid

conductivity (φ_s). A summary of heat sources in different layers of a PEMEC is presented in Table 7. The heat generation within the channels can be considered zero [26].

To determine the mass fraction of the species in the cell, one equation should be considered, which closely resembles Equation (16). If water evaporation is negligible, the species should be considered to be reduced to hydrogen and oxygen only. In this context, the mass fraction of hydrogen (Y_{H_2}) is determined by solving Equation (37) [26,107].

$$\nabla.\left(\rho_g f_g \varepsilon\, Y_{H_2} \tilde{u}_g\right) = \nabla.\left(\rho_g f_g \varepsilon\, D_m\, \nabla Y_{H_2}\right) + S_{H_2,cv} \tag{37}$$

where D_m and $S_{H_2,cv}$ are the mass diffusion coefficient and hydrogen mass crossover. The mass fraction of oxygen can be calculated simply by subtracting from 1.

- Mixture model

In this model, the two phases are treated as a single homogenous mixture with combined properties, including velocity ($\tilde{u}_m$), pressure (p_m), and temperature (T_m) [108]. Applying this technique significantly reduces the computational cost as the number of governing equations is halved [15,108]. The governing equations in the mixture model are derived by averaging on the Navier–Stokes equations. A separate continuity equation, along with a set of algebraic closure equations for relative velocities, is developed to calculate the volume fraction of the dispersed phase. [109]. Liquid water acts as the continuous phase, while gas is considered the dispersed phase. On the cathode side, the dispersed gas is a combination of hydrogen and water vapor, whereas on the anode side, hydrogen substitutes for oxygen in the mixture [15].

By defining two new parameters, namely the mass-averaged velocity ($\tilde{u}_m$) and mixture density (ρ_m), the continuity equation in the mixture model can be formulated, as shown in Equation (38) [108].

$$\nabla.\left(\rho_m \tilde{u}_m\right) = S_m \tag{38}$$

where ρ_m is calculated by the densities of the species with their corresponding volume fractions, as outlined in Equation (39).

$$\tilde{u}_m = \frac{1}{\rho_m}\sum_n f_n \rho_n\, \tilde{u}_n \tag{39}$$

where f_n, ρ_n, and $\tilde{u}_n$ are volume fraction, density, and the velocity vector of the active species in the flow. The mixture density (ρ_m) can be expressed by Equation (40) [15,108].

$$\rho_m = \sum_n f_n \rho_n \tag{40}$$

The momentum equation in the mixture model can be derived by combining the momentum equations (Equation (12)) for the continuous and dispersed phases in the flow [110]. The general form of the momentum equation in the mixture model is outlined as Equation (41) [15,16].

$$\nabla.\left(\rho_m \tilde{u}_m \tilde{u}_m\right) = -\nabla p + \nabla.\left(\tau_m\right) + \nabla.\left(\sum_n f_n \rho_n \tilde{u}_{dr,n}\; \tilde{u}_{dr,n}\right) + S_{mm} \tag{41}$$

where τ_m is the tension tensor for the mixture flow and can be expressed in terms of the mass-averaged velocity gradient (Equation (42)) [16,77]. S_{mm} represents the source term in the momentum equation.

$$\widetilde{\tau_m} = \mu_m\left[\nabla \tilde{u}_m + \left(\nabla \tilde{u}_m\right)^T\right] \tag{42}$$

where μ_m is the mixture's dynamic viscosity and can be expressed as Equation (43) [15,16,108].

$$\mu_m = \sum_n f_n \mu_n \tag{43}$$

The term $\tilde{u}_{dr,n}$ in Equation (41) denotes the drift velocity for the disperse phase n, calculated as the difference between the disperse phase velocity and the mixture velocity. ($\tilde{u}_{dr,n} = \tilde{u}_n - \tilde{u}_m$). Utilizing the same methodology, the energy and species transport equations can be derived for the mixture model, with comprehensive details provided in [15,108,110,111]. Recent advances in two-phase PEMEC modelling highlight the need for a balance between computational efficiency and physical accuracy. While Eulerian models provide detailed phase tracking, mixture models offer a computationally feasible alternative. Studies continue to refine these approaches by incorporating more realistic boundary conditions, improved mass transport considerations, and coupling with electrochemical simulations to enhance the predictive accuracy of PEMEC performance. After reviewing the governing equations for single-phase and two-phase models, it is useful to summarize the key trade-offs between these approaches. Table 9 provides a comparative analysis of single-phase and two-phase (Eulerian and mixture) models in terms of computational cost, accuracy, and suitability for different operating conditions. This comparison highlights the strengths and limitations of each method, assisting in the selection of an appropriate model for PEMEC simulations.

Table 9. Comparison of single-phase and two-phase models in PEMEC simulations, highlighting key trade-offs in cost, accuracy, and applicability.

Aspect	Single-Phase Model	Two-phase-Mixture Model	Two-Phase-Eulerian Model	Ref
Computational Cost	Low	Moderate	High	[112,113]
Accuracy in Gas–Liquid Interaction	Ignores two-phase effects	Approximates gas–liquid interaction	Fully resolves gas–liquid phases	[26,99,108]
Bubble Dynamics	Not modelled	Partially captured	Detailed bubble tracking	[4,104]
Best for Low/High-Current Densities	Best for low-current densities	Works for both low- and high-current densities	Best for high-current densities	[99,105,108]
Common Use Cases	Ideal for initial system analysis, simple performance estimation	Efficient for large-scale modelling, balancing accuracy and computational cost	Best for detailed local transport studies, high-fidelity research	[104,112,113]

To provide a clearer visual comparison, Figure 6 presents a bar chart illustrating the computational cost, accuracy, bubble dynamics, and suitability of each modelling approach at different current densities. This comparison (Table 9 and Figure 6) establishes the fundamental differences between single-phase and two-phase modelling approaches. However, these general trade-offs must be examined in more detail by analyzing specific performance outputs such as polarization plots, pressure distribution, velocity fields, and species volume fractions. The next section expands this analysis by comparing PEMEC simulation outputs from various models with experimental data.

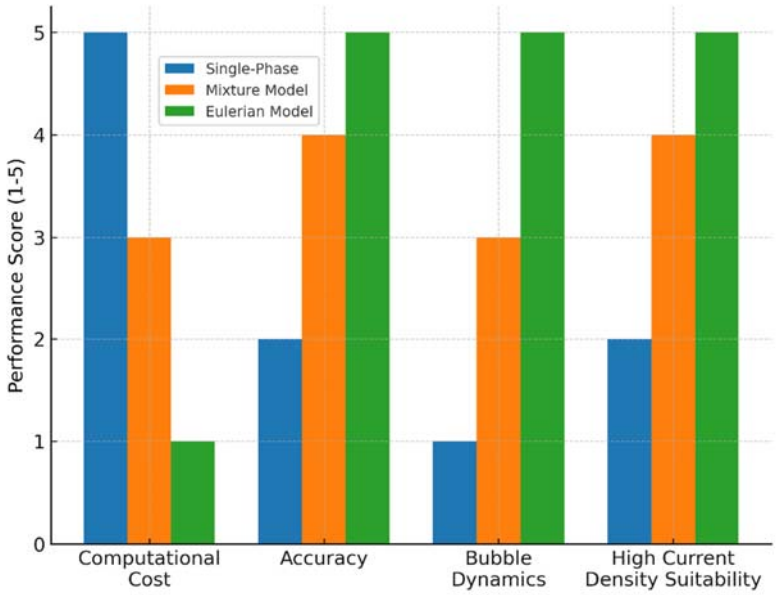

Figure 6. Comparative performance of single-phase and two-phase models in PEMEC simulations, evaluating computational cost, accuracy, bubble dynamics, and suitability at different current densities [26,27,30,108].

To complement the discussion above, Table 10 provides a summary of selected PEMEC simulation studies, highlighting the modelling approaches, software platforms, and notable features used in the literature.

Table 10. Common simulation platforms and modelling approaches in PEMEC studies.

Work	Year	Software Used	Model Type	Highlights/Remarks
Nie et al. [78]	2009	COMSOL multiphysics	Single-phase 3D	Flow-field analysis in bipolar plates
Ruiz et al. [102]	2021	ANSYS fluent	Single-phase 3D	Non-isothermal study at elevated temperature
Toghyani et al. [91]	2019	COMSOL multiphysics	Single-phase 3D	PTL and channel design optimization
Zinser et al. [103]	2023	COMSOL multiphysics	Two-phase	Anode-side water/oxygen transport study
Jiang et al. [26]	2023	COMSOL multiphysics	Two-phase Euler	Bubble detachment and drag force modelling
Tofighi et al. [79]	2025	Not specified	Electrical dynamics	Highlights system-level dynamic modelling gaps
Østenstad et al. [63]	2023	Not specified	Multiphysical model	Focus on membrane deformation and coupled physics

7. A Comparative Analysis Between the PEMEC Models

This section evaluates the performance of different PEMEC models by comparing key electrochemical and transport parameters. The analysis includes polarization plots, pressure distributions, velocity fields, and species volume fractions to assess the trade-offs in accuracy, computational cost, and physical realism. The results from different numerical studies are compared with experimental data, providing insights into how well each model captures real-world PEMEC behaviour.

A key benchmark for PEMEC models is their ability to reproduce polarization curves, which offer critical insights into electrochemical performance. Figure 7 presents a comparative analysis of polarization plots derived from a 0D model [17], a single-phase model [77], a two-phase mixture model [15], and experimental data [114]. These results, obtained

under similar operating conditions (80 °C and 1 atm), highlight the limitations of simpler models and the advantages of incorporating two-phase transport effects.

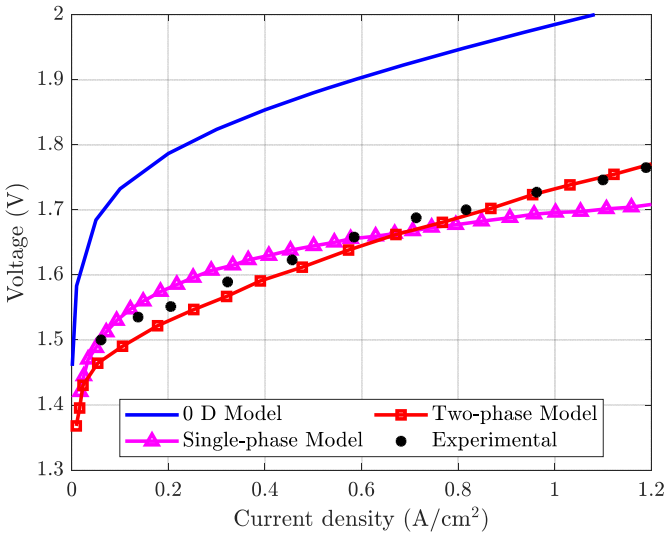

Figure 7. A comparison between the polarization plots of a PEMEC across different models: the 0D model, single-phase model, two-phase mixture model, and experimental data, all for an operating temperature of 80 °C and 1 atm [15,17,77,114].

The agreement between model predictions and experimental data depends on how well each model captures key transport phenomena, including gas evolution, bubble formation, and flow distribution. These effects become particularly significant at high-current densities, where single-phase models fail to represent real operating conditions accurately. To address these limitations, two-phase models—Eulerian and mixture-based approaches—are employed.

Both Eulerian and mixture models simulate gas–liquid interactions, but they differ in terms of accuracy and computational cost. The Eulerian model treats liquid and gas as separate phases, allowing for detailed bubble tracking but requiring substantial computational resources. The mixture model, on the other hand, assumes local phase equilibrium, approximating gas–liquid interactions with reduced complexity. While Eulerian models offer high-fidelity analysis, mixture models provide a practical alternative for large-scale simulations where phase separation effects are less dominant [14–16,26].

While polarization plots provide valuable electrochemical insights, they do not fully capture the transport dynamics within a PEMEC. Understanding how liquid and gas phases interact within the flow field is crucial for optimizing performance, particularly at high-current densities, where gas evolution significantly alters transport properties. To investigate these effects, several studies have compared single-phase and two-phase flow models within PEMEC half-cell domains—most notably those by Nie et al. [108], which provided key reference cases for evaluating gas–liquid interactions and their impact on cell performance. **As shown in Figure 8**, In their two-phase simulation of a PEMEC anode domain, they investigated pressure distribution and gas–liquid interactions using a mixture model approach. The study revealed a high-pressure region at the inlet and a lower-pressure outlet, with oxygen bubbles forming and influencing the transport properties along the channel. The reported pressure gradient ranged from 96 to 107 kPa, illustrating the critical influence of bubble dynamics on hydrodynamics and performance predictions.

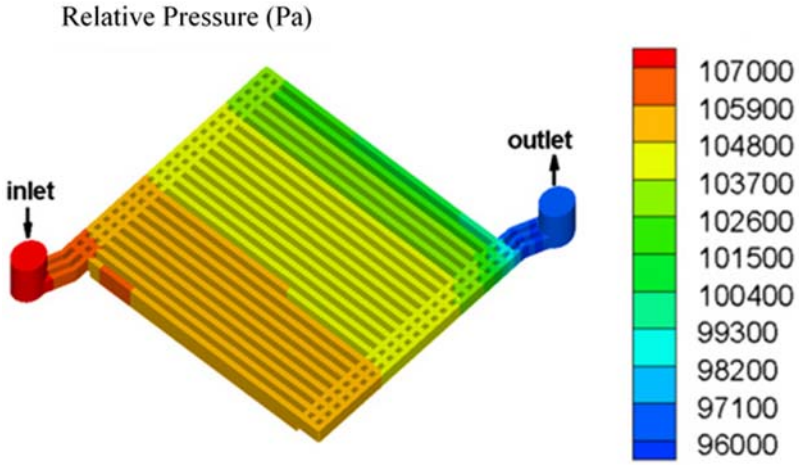

Figure 8. Original results extracted from [108], reproduced with permission from Elsevier, License No. 5974810501871. The figure presents the relative pressure distribution in the half-cell fluid domain for liquid water (continuous phase) and oxygen bubbles (dispersed phase), with 23 channels designed to enhance flow uniformity.

While pressure distribution provides insights into transport resistance and hydrodynamic performance, the volume fraction of water (H_2O) also plays a critical role in defining reactant availability, species transport, and electrochemical reaction efficiency. In PEMECs, oxygen bubble formation progressively reduces the local water concentration, affecting catalyst layer hydration, membrane conductivity, and overall transport properties. To explore this behaviour, Nie et al. [108] simulated the distribution of water volume fraction in a two-phase flow field. Their results, presented in Figure 9, revealed high water content at the inlet region (approximately 0.9–1.0), which gradually decreased along the channel length to around 0.5–0.6 at the outlet due to gas bubble formation. This spatial variation in water content highlights the transition from single-phase to two-phase flow and reinforces the importance of accurately modelling liquid–gas interactions in PEMECs.

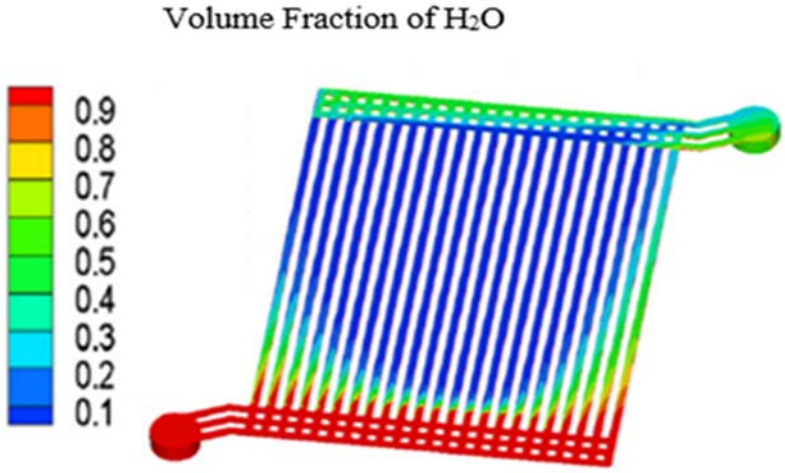

Figure 9. Original results extracted from [108], reproduced with permission from Elsevier, License No. 5974810501871. The figure illustrates the volume fraction distribution of water (H_2O) in the anode flow channels of a PEMEC during two-phase operation, showing progressive depletion of liquid water along the flow path due to oxygen evolution.

Beyond water distribution, oxygen evolution plays a crucial role in PEMEC operation, influencing reactant availability, pressure distribution, and overall system efficiency.

The accumulation of gas bubbles introduces additional transport resistance and alters local flow dynamics, making accurate modelling of oxygen volume fraction essential. Nie et al. [108] investigated this phenomenon through two-phase simulations using the mixture model, as shown in Figure 10. Their results revealed a clear trend: oxygen volume fraction begins near zero at the inlet—reflecting the absence of bubbles in the incoming liquid stream—and gradually increases along the flow field as electrochemical reactions proceed. By the outlet, the oxygen fraction reaches approximately 0.9–1.0 due to continuous gas generation and transport. This behaviour illustrates the dynamic impact of bubble formation on species transport and validates the importance of multiphase modelling in capturing PEMEC performance under realistic operating conditions.

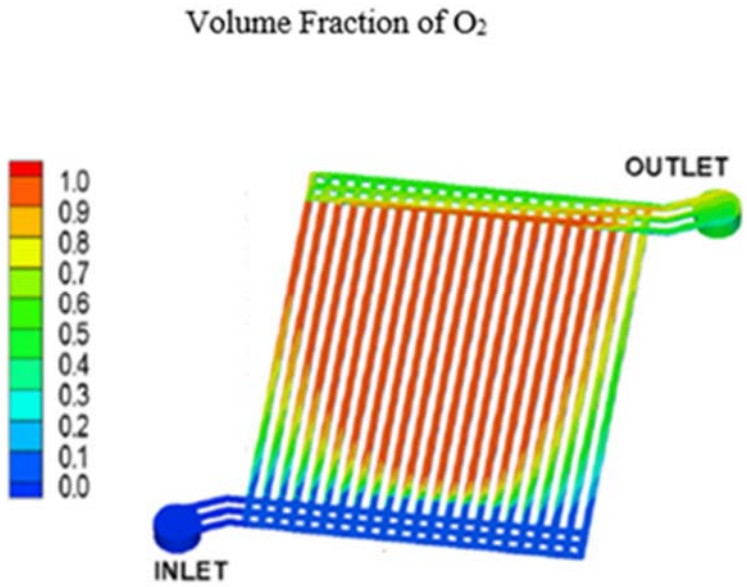

Figure 10. Original results extracted from [108], reproduced with permission from Elsevier, License No. 5974810501871. The figure shows the oxygen (O_2) volume fraction distribution in the anode flow channels of a PEMEC, highlighting the gradual gas-phase build up from inlet to outlet due to electrochemical reactions.

As shown in Figure 11, while the previous analyses focused on two-phase transport phenomena, it is also essential to evaluate single-phase flow conditions to establish a baseline for pressure distribution in PEMECs. Single-phase models, where only liquid water is present without gas evolution, provide insights into flow uniformity and pressure gradients in the absence of bubble-induced transport resistance. As reported by Nie et al. (2009) [78], single-phase simulations reveal a gradual decline in pressure from the inlet to the outlet under steady-state flow conditions, with liquid water introduced at a constant flow rate (e.g., 60 mL/min). These trends help isolate the fundamental hydrodynamic behaviour of the cell before introducing multiphase interactions. The observed pressure distribution serves as a computationally efficient reference for understanding flow resistance and guiding flow-field design in PEMECs.

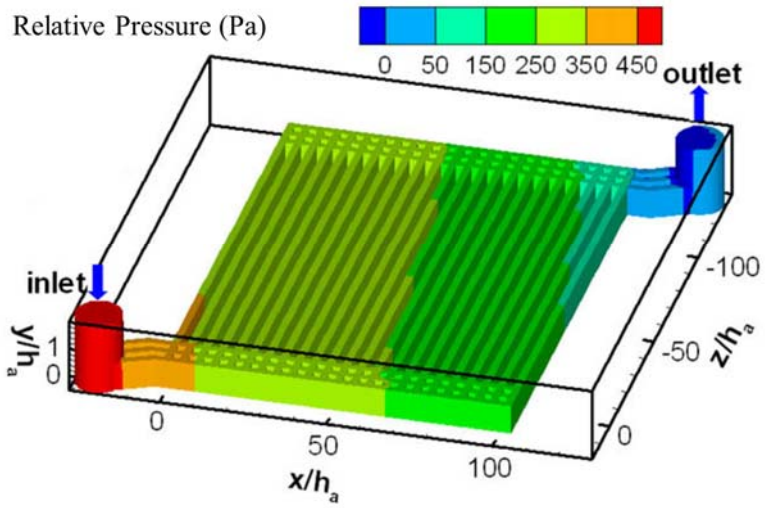

Figure 11. Single-phase pressure distribution in the anode flow field of a PEMEC with a water inlet flow rate of 60 mL/min. Original results extracted from Nie et al. [78], reproduced with permission from Elsevier.

By establishing this single-phase baseline, the impact of bubble formation and gas-phase interactions in two-phase models can be more effectively isolated and analyzed, leading to a deeper understanding of multiphase transport in PEMECs. While single-phase models provide valuable insights into pressure distribution and liquid flow dynamics, they fail to account for critical phenomena such as gas evolution, bubble-induced transport resistance, and phase separation, which significantly influence PEMEC performance at high-current densities. Previous studies [104,108] have demonstrated that neglecting two-phase effects leads to overly optimistic performance predictions and an underestimation of transport limitations, particularly in the anode flow field. Consequently, two-phase models have become the preferred approach for accurately capturing real-world PEMEC behaviour, as they incorporate gas–liquid interactions, bubble dynamics, and their impact on mass transport [99,105]. Nevertheless, single-phase models remain useful as a computationally efficient first step for parameter studies and design optimization, particularly at lower current densities, where gas evolution is minimal. The findings presented in this study further reinforce the necessity of multiphase modelling for high-fidelity simulations while demonstrating that single-phase models still serve as a valuable starting point for fundamental hydrodynamic analyses in PEMEC research.

8. Conclusions, and Future Research Directions

This review critically examined the advancements and challenges associated with proton exchange membrane electrolyzer cells (PEMECs), focusing on materials, system configurations, and numerical modelling approaches. The core research question addressed in this study was how improvements in electrocatalysts, flow-field designs, and computational simulations contribute to enhancing PEMEC efficiency, durability, and scalability. Through extensive analysis, key areas for optimization were identified, particularly in electrocatalyst development, flow-field design, and computational modelling.

Significant progress has been made in the development of high-efficiency catalysts and advanced membrane materials, yet the dependence on costly noble metals, particularly iridium, remains a major limitation. Addressing this issue requires further exploration of non-precious metal alternatives and nanostructured catalyst architectures, which have shown promise in reducing costs while maintaining electrochemical activity [114]. Additionally, innovative flow-field architectures, such as serpentine and interdigitated

designs, have demonstrated the potential to enhance reactant distribution and gas management, reducing mass transport losses and improving overall cell performance [78,108]. However, the scalability of these configurations remains an ongoing research challenge, particularly in large-scale PEMEC applications.

Computational modelling has become a crucial tool for predicting and optimizing PEMEC performance by offering insights into gas evolution, bubble dynamics, and electrochemical reactions. The application of two-phase flow models, such as Eulerian and mixture-based approaches, has provided a deeper understanding of multiphase interactions within PEMECs, including pressure distribution, velocity fields, and phase separation effects. The comparative analysis in this study confirmed that multiphase modelling significantly improves accuracy over single-phase models, reinforcing its importance in PEMEC research. While single-phase models serve as a useful hydrodynamic baseline, their inability to capture oxygen evolution and gas-phase interactions highlights the critical role of two-phase modelling in accurately predicting real-world PEMEC behaviour.

However, discrepancies between numerical predictions and experimental results highlight the need for further model validation to improve predictive accuracy and practical applicability [14,15]. Refining two-phase flow simulations remains a critical research area, particularly for improving PEMEC efficiency at high-current densities. As demonstrated in this study, bubble formation and gas evolution significantly impact flow resistance, reactant transport, and local pressure variations. While existing mixture models provide reasonable accuracy, further improvements are needed to accurately capture phase separation, electrolyte transport, and membrane hydration under dynamic conditions, which directly affect PEMEC efficiency and operational stability. Future research should integrate high-fidelity CFD simulations with experimental datasets to bridge this gap and refine model parameters based on real-world operating conditions. Despite significant advancements, challenges remain in developing cost-effective and durable catalysts, scalable electrode configurations, and experimentally validated numerical models. To address these challenges, future research should explore alternative catalyst compositions, refine electrode architectures, and leverage machine-learning-assisted modelling to optimize reaction kinetics, enhance transport properties, and improve predictive accuracy in numerical simulations. Furthermore, future research should prioritize establishing standardized experimental validation frameworks to ensure consistency and comparability across numerical models. The integration of in situ diagnostics, such as operando imaging or spectroscopy, could also offer deeper insight into dynamic behaviours like bubble evolution, flooding, and degradation. Exploring hybrid systems that combine PEMECs with real-time energy management platforms or smart control algorithms will be crucial for optimizing performance under fluctuating renewable energy conditions. These efforts will help bridge the gap between theoretical modelling and practical application, accelerating the commercialization of PEMEC technologies.

Additionally, improving membrane electrode assembly durability and refining two-phase flow simulations will be critical to better capturing real-world operating conditions. The integration of PEMECs with renewable energy sources necessitates optimized system control strategies to accommodate variable power inputs and ensure stable hydrogen production [1,3]. Overcoming these challenges is essential for advancing PEMEC technology toward widespread industrial deployment, ensuring its role as a cornerstone in the hydrogen economy.

By overcoming these barriers, PEMECs can be further optimized for industrial-scale hydrogen production, accelerating the transition toward a sustainable and decarbonized energy future. Continued advancements in catalyst engineering, membrane durability, and multiphysics modelling will be crucial to achieving this goal. Furthermore, integrating PEMECs with intermittent renewable energy sources requires improved system

control strategies to ensure stable and efficient operation under dynamic load conditions. This study provides a roadmap for future research, guiding the development of more efficient, durable, and economically viable PEM electrolyzers for green hydrogen production.

9. Study Limitations

This review acknowledges the following limitations:

- The computational trade-offs between accuracy and cost in two-phase models were not quantitatively analyzed due to space constraints.
- While a comprehensive overview of electrolysis methods and numerical models was provided, the absence of direct experimental validation limits the practical applicability of the findings.
- Certain complex electrochemical and multiphase flow phenomena were simplified for clarity, which may omit details relevant to real-world performance predictions.

Author Contributions: Conceptualization, S.C.S.; methodology, A.B.; software, A.B.; validation, A.B., P.K.D. and G.S.; formal analysis, A.B.; investigation, A.B.; resources, A.B.; data curation, A.B.; writing—original draft preparation, A.B.; writing—review and editing, P.K.D., G.S. and S.C.S.; visualization, A.B.; supervision, P.K.D., G.S. and S.C.S.; project administration, S.C.S. All authors have read and agreed to the published version of the manuscript.

Funding: This research received no external funding.

Acknowledgments: The authors acknowledge the computational resources provided by the High-Performance Computing Facility of the University of Technology Sydney. The first author, A.B., acknowledges the receipt of the UTS PhD scholarship for the pursuit of this study. All individuals and institutions mentioned have consented to this acknowledgment.

Conflicts of Interest: The authors declare that they have no known competing financial interests or personal relationships that could have appeared to influence the work reported in this paper.

Nomenclature

List of symbols

A	Surface area [m²]
C_j	Molar concentration of species j [mol/m³]
CCU	Carbon Capture and Utilization
CL	Catalyst layer
C_P	Specific heat at constant pressure [J/(kg K)]
D_j^0	Reference diffusivity of species j [m²/s]
D_j^{eff}	Effective diffusion coefficient of species j [m²/s]
D_m	Mass diffusion coefficient [m²/s]
d_P	Particle diameter of porous material [m]
F	Faraday's constant, 896,485.3 [C/mol]
f	Volume fraction in two-phase flow
GDE	Gas Diffusion Electrode
GDL	Gas diffusion layer
H^+	Proton
HER	Hydrogen evolution reaction
i	Current density [A/m²]
i_{a0}	Anode exchange current density [A/m²]
i_l	Proton current density in the membrane [A/m²]
i_s	Electron current density in the electrodes [A/m²]
K	Permeability of porous medium [m²]
k^{eff}	Effective thermal conductivity of the porous medium [W/(m K)]
k_f	Thermal conductivity of electrolyte [W/(m K)]

k_s	Thermal conductivity of solid [W/(m K)]
L_M	Membrane thickness [m]
M	Molecular weight of species [kg/mol]
MEA	Membrane electrode assembly
$\dot{N}$	Molar flow rate [mol/s]
OER	Oxygen evolution reaction
p	Pressure [Pa]
p^0	Reference pressure [Pa]
PEM	Proton exchange membrane
PEMEC	Proton exchange membrane electrolyzer cell
PEMFC	Proton exchange membrane fuel cell
PFSA	Perfluorosulfonic acid
PTL	Porous transport layer
R	Universal gas constant, 8.314 [J/(mol K)]
r	Interfacial resistance [Ω]
S_e	Source term for energy equation [W/m^3]
S_j	Source or sink term for species j [mol/(m^3 s)]
S_m	Source term in mass conservation equation [kg/(m^3 s)]
SOEC	Solid oxide electrolysis cell
S_u	Source term in momentum equation [N/m^3]
S_{wd}	Dissolved water [kg/(m^3 s)]
T	Temperature [C or K]
T_0	Reference temperature [C or K]
tor	Tortuosity
$\tilde{u}$	Velocity vector [m/s]
$\tilde{u}_{dr,n}$	Drift velocity for the disperse phase n [m/s]
V	Overall cell voltage [V]
V_0	Nernst potential [V]
Greek Symbols	
α	Transfer coefficient
ε	Porosity
η	Overpotential at electrode [V]
λ	Humidification degree
μ	Dynamic viscosity [Pa. s]
ρ	Density [kg/m^3]
σ	Electrical conductivity [S/m]
τ	Tension tensor [Pa]
φ	Electrical potential [V]
ω	Stoichiometric coefficient
Subscript and superscript	
a	Anode
c	Cathode
e	Energy
eff	Effective
g	Gas
j	Species
l	liquid
M	Membrane
m	Mixture of phases
n	The nth species
s	Solid
wd	Water dissolved

References

1. Rosen, M.A.; Koohi-Fayegh, S. The prospects for hydrogen as an energy carrier: An overview of hydrogen energy and hydrogen energy systems. *Energy Ecol. Environ.* **2016**, *1*, 10–29.
2. Qazi, U.Y. Future of hydrogen as an alternative fuel for next-generation industrial applications; challenges and expected opportunities. *Energies* **2022**, *15*, 4741.

3. Barbir, F. PEM electrolysis for production of hydrogen from renewable energy sources. *Sol. Energy* **2005**, *78*, 661–669.
4. Bessarabov, D.; Wang, H.; Li, H.; Zhao, N. *PEM Electrolysis for Hydrogen Production: Principles and Applications*; CRC Press: Boca Raton, FL, USA, 2016.
5. Das, P.K.; Jiao, K.; Wang, Y.; Barbir, F.; Li, X. *Fuel Cells for Transportation: Fundamental Principles and Applications*; Elsevier: Amsterdam, The Netherlands, 2023.
6. Ni, M.; Leung, D.Y.; Leung, M.K. A review on reforming bio-ethanol for hydrogen production. *Int. J. Hydrogen Energy* **2007**, *32*, 3238–3247.
7. Kayfeci, M.; Keçebaş, A.; Bayat, M. Hydrogen production. In *Solar Hydrogen Production*; Elsevier: Amsterdam, The Netherlands, 2019; pp. 45–83.
8. Al-Fatesh, A.S.; AL-Garadi, N.Y.; Osman, A.I.; Al-Mubaddel, F.S.; Ibrahim, A.A.; Khan, W.U.; Alanazi, Y.M.; Alrashed, M.M.; Alothman, O.Y. From plastic waste pyrolysis to Fuel: Impact of process parameters and material selection on hydrogen production. *Fuel* **2023**, *344*, 128107.
9. Rostrup-Nielsen, J.; Christiansen, L.J. *Concepts in Syngas Manufacture*; World Scientific: Singapore, 2011; Volume 10.
10. Incer-Valverde, J.; Korayem, A.; Tsatsaronis, G.; Morosuk, T. "Colors" of hydrogen: Definitions and carbon intensity. *Energy Convers. Manag.* **2023**, *291*, 117294.
11. Ajanovic, A.; Sayer, M.; Haas, R. The economics and the environmental benignity of different colors of hydrogen. *Int. J. Hydrogen Energy* **2022**, *47*, 24136–24154.
12. Carmo, M.; Fritz, D.L.; Mergel, J.; Stolten, D. A comprehensive review on PEM water electrolysis. *Int. J. Hydrogen Energy* **2013**, *38*, 4901–4934.
13. Sood, S.; Prakash, O.; Boukerdja, M.; Dieulot, J.-Y.; Ould-Bouamama, B.; Bressel, M.; Gehin, A.-L. Generic dynamical model of PEM electrolyser under intermittent sources. *Energies* **2020**, *13*, 6556.
14. Zheng, J.; Kang, Z.; Han, B.; Mo, J. Three-Dimensional Numerical Simulation of the Performance and Transport Phenomena of Oxygen Evolution Reactions in a Proton Exchange Membrane Water Electrolyzer. *Materials* **2023**, *16*, 1310.
15. Ma, Z.; Witteman, L.; Wrubel, J.A.; Bender, G. A comprehensive modeling method for proton exchange membrane electrolyzer development. *Int. J. Hydrogen Energy* **2021**, *46*, 17627–17643.
16. Corda, G.; Cucurachi, A.; Fontanesi, S.; d'Adamo, A. Three-Dimensional CFD Simulation of a Proton Exchange Membrane Electrolysis Cell. *Energies* **2023**, *16*, 5968.
17. Choi, P.; Bessarabov, D.G.; Datta, R. A simple model for solid polymer electrolyte (SPE) water electrolysis. *Solid State Ion.* **2004**, *175*, 535–539.
18. Xie, Z.; Yu, S.; Yang, G.; Li, K.; Ding, L.; Wang, W.; Cullen, D.A.; Meyer, H.M., III.; Retterer, S.T.; Wu, Z. Ultrathin platinum nanowire based electrodes for high-efficiency hydrogen generation in practical electrolyzer cells. *Chem. Eng. J.* **2021**, *410*, 128333.
19. Gittleman, C.S.; Coms, F.D.; Lai, Y.-H. Membrane durability: Physical and chemical degradation. In *Polymer Electrolyte Fuel Cell Degradation*; Academic Press: Cambridge, MA, USA, 2011; Volume 15.
20. Ogungbemi, E.; Ijaodola, O.; Khatib, F.N.; Wilberforce, T.; El Hassan, Z.; Thompson, J.; Ramadan, M.; Olabi, A.G. Fuel cell membranes–Pros and cons. *Energy* **2019**, *172*, 155–172.
21. Bui, J.C.; Davis, J.T.; Esposito, D.V. 3D-Printed electrodes for membraneless water electrolysis. *Sustain. Energy Fuels* **2020**, *4*, 213–225.
22. Ursua, A.; Gandia, L.M.; Sanchis, P. Hydrogen production from water electrolysis: Current status and future trends. *Proc. IEEE* **2011**, *100*, 410–426.
23. Hu, L.; Lindbergh, G.; Lagergren, C. Operating the nickel electrode with hydrogen-lean gases in the molten carbonate electrolysis cell (MCEC). *Int. J. Hydrogen Energy* **2016**, *41*, 18692–18698.
24. Wu, H.; Li, Z.; Ji, D.; Liu, Y.; Li, L.; Yuan, D.; Zhang, Z.; Ren, J.; Lefler, M.; Wang, B. One-pot synthesis of nanostructured carbon materials from carbon dioxide via electrolysis in molten carbonate salts. *Carbon* **2016**, *106*, 208–217.
25. Hauch, A.; Jensen, S.H.; Ramousse, S.; Mogensen, M. Performance and durability of solid oxide electrolysis cells. *J. Electrochem. Soc.* **2006**, *153*, A1741.
26. Jiang, Y.; Li, Y.; Ding, Y.; Hu, S.; Dang, J.; Yang, F.; Ouyang, M. Simulation and experiment study on two-phase flow characteristics of proton exchange membrane electrolysis cell. *J. Power Sources* **2023**, *553*, 232303.
27. Wang, W.; Han, B.; Cao, B.; Mo, J. Three-dimensional numerical simulation of bubble dynamics and design optimization of microchannel in proton exchange membrane water electrolyzers. *Int. J. Hydrogen Energy* **2023**, *48*, 36240–36253.
28. Berg, P.; Promislow, K.; Pierre, J.S.; Stumper, J.; Wetton, B. Water management in PEM fuel cells. *J. Electrochem. Soc.* **2004**, *151*, A341.

29. Diaz, D.F.R.; Valenzuela, E.; Wang, Y. A component-level model of polymer electrolyte membrane electrolysis cells for hydrogen production. *Appl. Energy* **2022**, *321*, 119398.
30. Kalinnikov, A.; Grigoriev, S.; Bessarabov, D.; Bouzek, K. Two-phase mass transfer in porous transport layers of the electrolysis cell based on a polymer electrolyte membrane: Analysis of the limitations. *Electrochim. Acta* **2021**, *387*, 138541.
31. Liu, C. Noble Metal Coated Porous Transport Layers for Polymer Electrolyte Membrane Water Electrolysis. Ph.D. Thesis, Rheinisch-Westfälische Technische Hochschule Aachen, Aachen, Germany, 2021.
32. Millet, P.; Mbemba, N.; Grigoriev, S.; Fateev, V.; Aukauloo, A.; Etiévant, C. Electrochemical performances of PEM water electrolysis cells and perspectives. *Int. J. Hydrogen Energy* **2011**, *36*, 4134–4142.
33. Smolinka, T.; Bergmann, H.; Garche, J.; Kusnezoff, M. The history of water electrolysis from its beginnings to the present. In *Electrochemical Power Sources: Fundamentals, Systems, and Applications*; Elsevier: Amsterdam, The Netherlands, 2022; pp. 83–164.
34. Thumbarathy, D.; Gupta, G.; Mamlouk, M.; Das, P.K. Fabrication and characterization of tuneable flow-channel/gas-diffusion-layer interface for polymer electrolyte fuel cells. *J. Electrochem. Energy Convers. Storage* **2020**, *17*, 011010.
35. Kang, Z.; Yu, S.; Yang, G.; Li, Y.; Bender, G.; Pivovar, B.S.; Green, J.B., Jr.; Zhang, F.-Y. Performance improvement of proton exchange membrane electrolyzer cells by introducing in-plane transport enhancement layers. *Electrochim. Acta* **2019**, *316*, 43–51.
36. Dönitz, W.; Erdle, E. High-temperature electrolysis of water vapor—Status of development and perspectives for application. *Int. J. Hydrogen Energy* **1985**, *10*, 291–295.
37. Mališ, J.; Mazúr, P.; Paidar, M.; Bystron, T.; Bouzek, K. Nafion 117 stability under conditions of PEM water electrolysis at elevated temperature and pressure. *Int. J. Hydrogen Energy* **2016**, *41*, 2177–2188.
38. Ding, L.; Xie, Z.; Yu, S.; Wang, W.; Terekhov, A.Y.; Canfield, B.K.; Capuano, C.B.; Keane, A.; Ayers, K.; Cullen, D.A. Electrochemically Grown Ultrathin Platinum Nanosheet Electrodes with Ultralow Loadings for Energy-Saving and Industrial-Level Hydrogen Evolution. *Nano-Micro Lett.* **2023**, *15*, 144.
39. Pehlivan-Davis, S. Polymer Electrolyte Membrane (PEM) Fuel Cell Seals Durability. Ph.D. Dissertation, Loughborough University, Loughborough, UK, 2016.
40. Park, S.; Popov, B.N. Effect of a GDL based on carbon paper or carbon cloth on PEM fuel cell performance. *Fuel* **2011**, *90*, 436–440.
41. Ubong, E.; Shi, Z.; Wang, X. Three-dimensional modeling and experimental study of a high temperature PBI-based PEM fuel cell. *J. Electrochem. Soc.* **2009**, *156*, B1276.
42. Dillard, D.A.; Guo, S.; Ellis, M.W.; Lesko, J.J.; Dillard, J.G.; Sayre, J.; Vijayendran, B. Seals and sealants in PEM fuel cell environments: Material, design, and durability challenges. In Proceedings of the International Conference on Fuel Cell Science, Engineering and Technology, Rochester, NY, USA, 14–16 June 2004.
43. Hermann, A.; Chaudhuri, T.; Spagnol, P. Bipolar plates for PEM fuel cells: A review. *Int. J. Hydrogen Energy* **2005**, *30*, 1297–1302.
44. Santamaria, A.D.; Das, P.K. Liquid water transport and management for fuel cells. In *Fuel Cells for Transportation*; Elsevier: Amsterdam, The Netherlands, 2023; pp. 225–251.
45. Li, P.; Ki, J.-P.; Liu, H. Analysis and optimization of current collecting systems in PEM fuel cells. *Int. J. Energy Environ. Eng.* **2012**, *3*, 2.
46. Kim, J.; Kim, H.E.; Lee, H. Single-atom catalysts of precious metals for electrochemical reactions. *ChemSusChem* **2018**, *11*, 104–113.
47. Gao, H.; Jiang, Y.; Chen, R.; Dong, C.L.; Huang, Y.C.; Ma, M.; Shi, Z.; Liu, J.; Zhang, Z.; Qiu, M. Alloyed Pt Single-Atom Catalysts for Durable PEM Water Electrolyzer. *Adv. Funct. Mater.* **2023**, *33*, 2214795.
48. Ding, L.; Wang, W.; Xie, Z.; Li, K.; Yu, S.; Capuano, C.B.; Keane, A.; Ayers, K.; Zhang, F.-Y. Highly Porous Iridium Thin Electrodes with Low Loading and Improved Reaction Kinetics for Hydrogen Generation in PEM Electrolyzer Cells. *ACS Appl. Mater. Interfaces* **2023**, *15*, 24284–24295.
49. Siracusano, S.; Baglio, V.; Grigoriev, S.; Merlo, L.; Fateev, V.; Aricò, A. The influence of iridium chemical oxidation state on the performance and durability of oxygen evolution catalysts in PEM electrolysis. *J. Power Sources* **2017**, *366*, 105–114.
50. Roberson, S.; Finello, D.; Davis, R. Electrochemical evaluation of molybdenum nitride electrodes in H_2SO_4 electrolyte. *J. Appl. Electrochem.* **1999**, *29*, 75–80.
51. Mo, J.; Steen, S.; Kang, Z.; Yang, G.; Taylor, D.A.; Li, Y.; Toops, T.J.; Brady, M.P.; Retterer, S.T.; Cullen, D.A. Study on corrosion migrations within catalyst-coated membranes of proton exchange membrane electrolyzer cells. *Int. J. Hydrogen Energy* **2017**, *42*, 27343–27349.
52. Ampurdanés, J.; Chourashiya, M.; Urakawa, A. Cobalt oxide-based materials as non-PGM catalyst for HER in PEM electrolysis and in situ XAS characterization of its functional state. *Catal. Today* **2019**, *336*, 161–168.

53. Othman, R.; Dicks, A.L.; Zhu, Z. Non precious metal catalysts for the PEM fuel cell cathode. *Int. J. Hydrogen Energy* **2012**, *37*, 357–372.
54. Bu, Y.; Wang, Y.; Han, G.F.; Zhao, Y.; Ge, X.; Li, F.; Zhang, Z.; Zhong, Q.; Baek, J.B. Carbon-based electrocatalysts for efficient hydrogen peroxide production. *Adv. Mater.* **2021**, *33*, 2103266.
55. Wang, Y.; Diaz, D.F.R.; Chen, K.S.; Wang, Z.; Adroher, X.C. Materials, technological status, and fundamentals of PEM fuel cells–a review. *Mater. Today* **2020**, *32*, 178–203.
56. Thuc, V.D.; Tinh, V.D.C.; Kim, D. Simultaneous improvement of proton conductivity and chemical stability of Nafion membranes via embedment of surface-modified ceria nanoparticles in membrane surface. *J. Membr. Sci.* **2022**, *642*, 119990.
57. Ito, H.; Maeda, T.; Nakano, A.; Takenaka, H. Properties of Nafion membranes under PEM water electrolysis conditions. *Int. J. Hydrogen Energy* **2011**, *36*, 10527–10540.
58. Chae, K.-J.; Kim, K.-Y.; Choi, M.-J.; Yang, E.; Kim, I.S.; Ren, X.; Lee, M. Sulfonated polyether ether ketone (SPEEK)-based composite proton exchange membrane reinforced with nanofibers for microbial electrolysis cells. *Chem. Eng. J.* **2014**, *254*, 393–398.
59. Jang, I.-Y.; Kweon, O.-H.; Kim, K.-E.; Hwang, G.-J.; Moon, S.-B.; Kang, A.-S. Covalently cross-linked sulfonated poly (ether ether ketone)/tungstophosphoric acid composite membranes for water electrolysis application. *J. Power Sources* **2008**, *181*, 127–134.
60. Lv, B.; Yin, H.; Shao, Z.; Luan, Z.; Huang, Z.; Sun, S.; Teng, Y.; Miu, C.; Gao, Q. Novel polybenzimidazole/graphitic carbon nitride nanosheets composite membrane for the application of acid-alkaline amphoteric water electrolysis. *J. Energy Chem.* **2022**, *64*, 607–614.
61. Wan, L.; Xu, Z.; Wang, P.; Lin, Y.; Wang, B. H_2SO_4-doped polybenzimidazole membranes for hydrogen production with acid-alkaline amphoteric water electrolysis. *J. Membr. Sci.* **2021**, *618*, 118642.
62. Lee, H.-O.; Yesuraj, J.; Kim, K. Parametric study to optimize proton exchange membrane electrolyzer cells. *Appl. Energy* **2022**, *314*, 118928.
63. Østenstad, J. Multiphysical modeling of a next generation PEM electrolyser. 2023. Available online: https://hdl.handle.net/11250/3100125 (accessed on 15 February 2025).
64. Thangarasu, S.; Oh, T.H. Progress in poly (phenylene oxide) based cation exchange membranes for fuel cells and redox flow batteries applications. *Int. J. Hydrogen Energy* **2021**, *46*, 38381–38415.
65. Feng, Z. Investigation of Polyphenylene Oxide-Based Membranes for Anion Exchange Water Electrolyser. Ph.D. Dissertation, Newcastle University, Newcastle upon Tyne, UK, 2022.
66. Bender, J.; Mayerhöfer, B.; Trinke, P.; Bensmann, B.; Hanke-Rauschenbach, R.; Krajinovic, K.; Thiele, S.; Kerres, J. H^+-conducting aromatic multiblock copolymer and blend membranes and their application in pem electrolysis. *Polymers* **2021**, *13*, 3467.
67. Goni-Urtiaga, A.; Presvytes, D.; Scott, K. Solid acids as electrolyte materials for proton exchange membrane (PEM) electrolysis. *Int. J. Hydrogen Energy* **2012**, *37*, 3358–3372.
68. Shah, M.R.; Zulfqar, M.; Khan, Z.S. Inorganic-Organic Nano Composite Hybrid Membrane Based on Titania and Polystyrene for High Temperature PEM Fuel Cell. Ph.D. Dissertation, National University of Science and Technology, Bulawayo, Zimbabwe, 2018.
69. Henkensmeier, D.; Najibah, M.; Harms, C.; Žitka, J.; Hnát, J.; Bouzek, K. Overview: State-of-the art commercial membranes for anion exchange membrane water electrolysis. *J. Electrochem. Energy Convers. Storage* **2021**, *18*, 024001.
70. Khalid, H.; Najibah, M.; Park, H.S.; Bae, C.; Henkensmeier, D. Properties of anion exchange membranes with a focus on water electrolysis. *Membranes* **2022**, *12*, 989.
71. Pushkareva, I.; Pushkarev, A.; Grigoriev, S.; Modisha, P.; Bessarabov, D. Comparative study of anion exchange membranes for low-cost water electrolysis. *Int. J. Hydrogen Energy* **2020**, *45*, 26070–26079.
72. Xing, L.; Xuan, J.; Das, P.K. Fuel cell fundamentals. In *Fuel Cells for Transportation*; Elsevier: Amsterdam, The Netherlands, 2023; pp. 29–72.
73. Barbir, F. PEM fuel cells. In *Fuel Cell Technology: Reaching Towards Commercialization*; Springer: Berlin/Heidelberg, Germany, 2006; pp. 27–51.
74. Litster, S.; McLean, G. PEM fuel cell electrodes. *J. Power Sources* **2004**, *130*, 61–76.
75. Schröder, J.; Mints, V.A.; Bornet, A.; Berner, E.; Fathi Tovini, M.; Quinson, J.; Wiberg, G.K.; Bizzotto, F.; El-Sayed, H.A.; Arenz, M. The gas diffusion electrode setup as straightforward testing device for proton exchange membrane water electrolyzer catalysts. *JACS Au* **2021**, *1*, 247–251.
76. Yang, R.; Mohamed, A.; Kim, K. Optimal design and flow-field pattern selection of proton exchange membrane electrolyzers using artificial intelligence. *Energy* **2023**, *264*, 126135.

77. Toghyani, S.; Afshari, E.; Baniasadi, E. Metal foams as flow distributors in comparison with serpentine and parallel flow fields in proton exchange membrane electrolyzer cells. *Electrochim. Acta* **2018**, *290*, 506–519.
78. Nie, J.; Chen, Y.; Cohen, S.; Carter, B.D.; Boehm, R.F. Numerical and experimental study of three-dimensional fluid flow in the bipolar plate of a PEM electrolysis cell. *Int. J. Therm. Sci.* **2009**, *48*, 1914–1922.
79. Tofighi-Milani, M.; Fattaheian-Dehkordi, S.; Lehtonen, M. Electrolysers: A Review on Trends, Electrical Modeling, and Their Dynamic Responses. *IEEE Access* **2025**, *13*, 39870–39885.
80. Radhakrishnan, V.; Haridoss, P. Differences in structure and property of carbon paper and carbon cloth diffusion media and their impact on proton exchange membrane fuel cell flow field design. *Mater. Des.* **2011**, *32*, 861–868.
81. Wang, L.; Husar, A.; Zhou, T.; Liu, H. A parametric study of PEM fuel cell performances. *Int. J. Hydrogen Energy* **2003**, *28*, 1263–1272.
82. Das, P.K.; Grippin, A.; Kwong, A.; Weber, A.Z. Liquid-water-droplet adhesion-force measurements on fresh and aged fuel-cell gas-diffusion layers. *J. Electrochem. Soc.* **2012**, *159*, B489.
83. Li, Y.; Li, Z.; Lei, L.; Lan, T.; Li, Y.; Li, P.; Lin, X.; Liu, R.; Huang, Z.; Fen, X. Chemical vapor deposition-grown carbon nanotubes/graphene hybrids for electrochemical energy storage and conversion. *FlatChem* **2019**, *15*, 100091.
84. Kumar, S.S.; Himabindu, V. Boron-Doped Carbon nanoparticles supported palladium as an efficient hydrogen evolution electrode in PEM water electrolysis. *Renew. Energy* **2020**, *146*, 2281–2290.
85. Nørskov, J.K.; Bligaard, T.; Logadottir, A.; Kitchin, J.; Chen, J.G.; Pandelov, S.; Stimming, U. Trends in the exchange current for hydrogen evolution. *J. Electrochem. Soc.* **2005**, *152*, J23.
86. Medford, A.J.; Vojvodic, A.; Hummelshøj, J.S.; Voss, J.; Abild-Pedersen, F.; Studt, F.; Bligaard, T.; Nilsson, A.; Nørskov, J.K. From the Sabatier principle to a predictive theory of transition-metal heterogeneous catalysis. *J. Catal.* **2015**, *328*, 36–42.
87. Butler, K.T.; Davies, D.W.; Cartwright, H.; Isayev, O.; Walsh, A. Machine learning for molecular and materials science. *Nature* **2018**, *559*, 547–555.
88. Chandesris, M.; Médeau, V.; Guillet, N.; Chelghoum, S.; Thoby, D.; Fouda-Onana, F. Numerical modelling of membrane degradation in PEM water electrolyzer: Influence of the temperature and current density. *Int. J. Hydrogen Energy* **2015**, *40*, 1–8.
89. Toghyani, S.; Afshari, E.; Baniasadi, E.; Atyabi, S. Thermal and electrochemical analysis of different flow field patterns in a PEM electrolyzer. *Electrochim. Acta* **2018**, *267*, 234–245.
90. Stiber, S.; Sata, N.; Morawietz, T.; Ansar, S.; Jahnke, T.; Lee, J.K.; Bazylak, A.; Fallisch, A.; Gago, A.; Friedrich, K.A. A high-performance, durable and low-cost proton exchange membrane electrolyser with stainless steel components. *Energy Environ. Sci.* **2022**, *15*, 109–122.
91. Toghyani, S.; Afshari, E.; Baniasadi, E. Three-dimensional computational fluid dynamics modeling of proton exchange membrane electrolyzer with new flow field pattern. *J. Therm. Anal. Calorim.* **2019**, *135*, 1911–1919.
92. Mohamed, A.; Ibrahem, H.; Kim, K. Machine learning-based simulation for proton exchange membrane electrolyzer cell. *Energy Rep.* **2022**, *8*, 13425–13437.
93. Bard, A.J.; Faulkner, L.R.; White, H.S. *Electrochemical Methods: Fundamentals and Applications*; John Wiley & Sons: Hoboken, NJ, USA, 2022.
94. Bockris, J.; Reddy, A.M. *Gamboa-Aldeco in:"Modern Electrochemistry Vol. 2A"*; Kluwer Academic/Plenum Publishers: New York, NY, USA, 2000.
95. Millet, P. Water electrolysis using eme technology: Electric potential distribution inside a nafion membrane during electrolysis. *Electrochim. Acta* **1994**, *39*, 2501–2506.
96. Ramousse, J.; Didierjean, S.; Lottin, O.; Maillet, D. Estimation of the effective thermal conductivity of carbon felts used as PEMFC Gas Diffusion Layers. *Int. J. Therm. Sci.* **2008**, *47*, 1–6.
97. Das, P.K.; Li, X.; Liu, Z.-S. Effective transport coefficients in PEM fuel cell catalyst and gas diffusion layers: Beyond Bruggeman approximation. *Appl. Energy* **2010**, *87*, 2785–2796.
98. Um, S.; Wang, C.Y.; Chen, K. Computational fluid dynamics modeling of proton exchange membrane fuel cells. *J. Electrochem. Soc.* **2000**, *147*, 4485.
99. Han, B.; Mo, J.; Kang, Z.; Zhang, F.-Y. Effects of membrane electrode assembly properties on two-phase transport and performance in proton exchange membrane electrolyzer cells. *Electrochim. Acta* **2016**, *188*, 317–326.
100. Vafai, K. *Handbook of Porous Media*; CRC Press: Boca Raton, FL, USA, 2015.
101. Skripkin, E. Effective Thermal Conductivity of Porous Media: An Integrated Approach. Master's Thesis, University of Calgary, Calgary, AB, Canada, 2015.

102. Ruiz, D.D.H.; Sasmito, A.P.; Shamim, T. Numerical investigation of the high temperature PEM electrolyzer: Effect of flow channel configurations. *ECS Trans.* **2013**, *58*, 99.
103. Zinser, A.; Papakonstantinou, G.; Sundmacher, K. Analysis of mass transport processes in the anodic porous transport layer in PEM water electrolysers. *Int. J. Hydrogen Energy* **2019**, *44*, 28077–28087.
104. Arbabi, F.; Montazeri, H.; Abouatallah, R.; Wang, R.; Bazylak, A. Three-dimensional computational fluid dynamics modelling of oxygen bubble transport in polymer electrolyte membrane electrolyzer porous transport layers. *J. Electrochem. Soc.* **2016**, *163*, F3062.
105. Wang, Z.; Xu, C.; Wang, X.; Liao, Z.; Du, X. Numerical investigation of water and temperature distributions in a proton exchange membrane electrolysis cell. *Sci. China Technol. Sci.* **2021**, *64*, 1555–1566.
106. White, F.M.; Majdalani, J. *Viscous Fluid Flow*; McGraw-Hill: New York, NY, USA, 2006; Volume 3.
107. Fluent, A. *Ansys Fluent Theory Guide*; Ansys Inc.: Canonsburg, PA, USA, 2011; Volume 15317, pp. 724–746.
108. Nie, J.; Chen, Y. Numerical modeling of three-dimensional two-phase gas–liquid flow in the flow field plate of a PEM electrolysis cell. *Int. J. Hydrogen Energy* **2010**, *35*, 3183–3197.
109. Tijani, A.S.; Rahim, A.A. Numerical modeling the effect of operating variables on Faraday efficiency in PEM electrolyzer. *Procedia Technol.* **2016**, *26*, 419–427.
110. Manninen, M.; Taivassalo, V.; Kallio, S. *On the Mixture Model for Multiphase Flow*; Technical Research Centre of Finland: Espoo, Finland, 1996.
111. Ishii, M.; Mishima, K. Two-fluid model and hydrodynamic constitutive relations. *Nucl. Eng. Des.* **1984**, *82*, 107–126.
112. Abdin, Z.; Webb, C.; Gray, E.M. Modelling and simulation of a proton exchange membrane (PEM) electrolyser cell. *Int. J. Hydrogen Energy* **2015**, *40*, 13243–13257.
113. Chen, Z.; Yin, L.; Wang, Z.; Wang, K.; Ye, F.; Xu, C. Numerical simulation of parameter change in a proton exchange membrane electrolysis cell based on a dynamic model. *Int. J. Energy Res.* **2022**, *46*, 24074–24090.
114. Debe, M.; Hendricks, S.; Vernstrom, G.; Meyers, M.; Brostrom, M.; Stephens, M.; Chan, Q.; Willey, J.; Hamden, M.; Mittelsteadt, C.K. Initial performance and durability of ultra-low loaded NSTF electrodes for PEM electrolyzers. *J. Electrochem. Soc.* **2012**, *159*, K165.